

The fractional virial potential energy in two-component systems

R. Caimmi^{*}, T. Valentinuzzi[†]

June 9, 2008

Abstract

Two-component systems are conceived as macrogases, and the related equation of state is expressed using the virial theorem for sub-systems, under the restriction of homeoidally striated density profiles. Explicit calculations are performed for a useful reference case and a few cases of astrophysical interest, both with and without truncation radius. Shallower density profiles are found to yield an equation of state, $\phi = \phi(y, m)$, characterized (for assigned values of the fractional mass, $m = M_j/M_i$) by the occurrence of two extremum points, a minimum and a maximum, as found in an earlier attempt. Steeper density profiles produce a similar equation of state, which implies that a special value of m is related to a critical curve where the above mentioned extremum points reduce to a single horizontal inflexion point, and curves below the critical one show no extremum points. The similarity of the isofractional mass curves to van der Waals' isothermal curves, suggests the possibility of a phase transition in a bell-shaped region of the $(Oy\phi)$ plane, where the fractional truncation radius along a selected direction is $y = R_j/R_i$, and the fractional virial potential energy is $\phi = (E_{ji})_{\text{vir}}/(E_{ij})_{\text{vir}}$. Further investigation is devoted to mass distributions described by Hernquist (1990) density profiles, for which

^{*}*Astronomy Department, Padua Univ., Vicolo Osservatorio 2, I-35122 Padova, Italy*
email: roberto.caimmi@unipd.it fax: 39-049-8278212

[†]*Astronomy Department, Padua Univ., Vicolo Osservatorio 2, I-35122 Padova, Italy*
email: tiziano.valentinuzzi@unipd.it fax: 39-049-8278212

an additional relation can be used to represent a sample of $N = 16$ elliptical galaxies (EGs) on the $(Oy\phi)$ plane. Even if the evolution of elliptical galaxies and their hosting dark matter (DM) haloes, in the light of the model, has been characterized by equal fractional mass, m , and equal scaled truncation radius, or concentration, $\Xi_u = R_u/r_u^\dagger$, $u = i, j$, still it cannot be considered as strictly homologous, due to different values of fractional truncation radii, y , or fractional scaling radii, $y^\dagger = r_j^\dagger/r_i^\dagger$, deduced from sample objects.

keywords - *galaxies: evolution* - *dark matter: haloes*.

1 Introduction

Ordinary fluids (e.g., gases and liquids) may be bounded by rigid walls which allow particle number conservation, avoiding evaporation. Macroscopical parameters (pressure, density, and temperature) remain uniform within the box, due to its reduced dimensions. On the other hand, astrophysical fluids (e.g., stars and galaxies) may be conceived as bounded by “gravitational” walls which violate particle number conservation by allowing evaporation. The macroscopical parameters exhibit gradients because they cannot remain uniform within the “gravitational” box, due to its large-scale dimensions.

In particular, sufficiently extended celestial objects show at least two distinct components: core-envelope for stars, core-halo for elliptical galaxies, bulge-disk for spiral and lenticular galaxies, baryonic-nonbaryonic for virialized (matter) density perturbations, and matter-dark energy for virialized (matter + dark energy) density perturbations. On this basis, an investigation on two-component astrophysical fluids appears useful for the comprehension and the interpretation of what is inferred from observations. To this aim, the choice of the density profiles is of basic importance. The laws of ideal and real gases were deduced from ordinary fluids, characterized by uniform density profiles. Accordingly, it is expected that astrophysical fluid laws are related to the specified density profiles, and different laws hold for different matter distributions.

Strictly speaking, a density profile should be deduced from the distribution function, or vice versa. Unfortunately, the determination of the distribution function is much more difficult than in one-component systems, and only a few cases have been studied in detail at present (e.g., Ciotti, 1996, 1999). On the other hand, global properties exhibited by simple density profiles (with somewhere negative distribution function) are expected to maintain a similar trend in dealing with much more complex density profiles (with nonnegative distribution function).

As the current attempt is mainly aimed to explore global properties instead of local properties, density profiles shall be selected according to their intrinsic simplicity, regardless from the physical meaning of the distribution function. Configurations described by simple density profiles could be sufficiently close to their counterparts described by self-consistent density profiles, and related results hold to a first extent. In any case, the self-consistency of density profiles with respect to nonnegativity of the distribution function, can be checked using a specific theorem (Ciotti and Pellegrini, 1992).

To a first extent, the particle number shall be supposed to be conserved, which is equivalent to conceive the boundary of each subsystem as a perfectly reflecting surface in order to avoid evaporation. In this view, a possible choice of macroscopical parameters is: the fractional virial potential energy, ϕ ; the fractional truncation radius, y ; and the fractional mass, m ; as done in a pioneering paper with respect to uniform density profiles i.e. homogeneous configurations (Caimmi and Secco, 1990, hereafter quoted as CS90). Accordingly, each subsystem is supposed to be virialized, in the sense that the virial equations are satisfied by averaging over a sufficiently long time, and particles move within a bounded region (e.g., Landau and Lifchitz, 1966, Chap. II, §10; Caimmi, 2007a). Then virial equilibrium is a necessary (but not sufficient) condition for dynamical or hydrostatic equilibrium, which, on the other hand, does not imply pressureless configurations, as the stress tensor is related to the kinetic-energy tensor (e.g., Binney and Tremaine, 1987, Chap. 4, §2).

For sake of simplicity, the applications of the general theory shall be restricted to homeoidally striated density profiles (e.g., Roberts, 1962; Caimmi, 1993; Caimmi and Marmo, 2003, hereafter quoted as CM03). The larger effects of asphericity are expected to occur in homogeneous configurations, which have widely been investigated (Brosche et al., 1983; Caimmi et al., 1984; CS90; Caimmi and Secco, 1992). Focaloidally striated density profiles involve far larger difficulty (e.g., Caimmi, 1995, 2003).

The current investigation is mainly devoted to the following points: (i) expression of an equation of state for two-component systems; (ii) description of global properties deduced from selected density profiles; and (iii) application to elliptical galaxies belonging to a restricted sample, to be represented on the $(Oy\phi)$ plane, for fiducial values of model parameters.

The work is organized as follows. The basic theory of two-component systems with homeoidally striated density profiles, is reviewed and extended (to include both cored and cuspy matter distributions) in Section 2. The particularization to selected density profiles, involving explicit expressions, is made in Section 3. The results and related global properties are described and discussed in Section 4. Elliptical galaxies belonging to a restricted sample,

are represented on the $(Oy\phi)$ plane, for fiducial values of model parameters, in Section 5, where some considerations are drawn. The concluding remarks are reported in Section 6.

2 Basic theory

A general theory of two-component matter distributions has been exhaustively treated in an earlier paper (Caimmi and Secco, 1992), and the interested reader is addressed therein and in parent investigations (MacMillan, 1930, Chap.III, §76; Limber, 1959; Neutsch, 1979; Brosche et al., 1983; Caimmi et al., 1984) for further details. What is relevant for the current attempt, shall be reviewed and extended. If not otherwise stated, matter distributions should be conceived as continuous media instead of discrete particle sets (e.g., Limber, 1959; Caimmi, 2007a). In the following, general definitions and related explicit expressions will be provided. Readers mainly interested to a simple reference case and a few cases of astrophysical interest, might directly go to Section 3, while readers mainly interested to the results and an application to elliptical galaxies, might directly go to Sections 4 and 5, respectively.

2.1 Kinetic-energy and self potential-energy tensors

For an assigned density profile, the kinetic-energy tensor and the kinetic energy read (Binney and Tremaine, 1987, Chap. 4, §4.3):

$$(E_{\text{kin}})_{pq} = \frac{1}{2} \int_S \rho(x_1, x_2, x_3) v_p v_q d^3S \quad ; \quad p = 1, 2, 3 \quad ; \quad q = 1, 2, 3 \quad ; \quad (1a)$$

$$E_{\text{kin}} = \frac{1}{2} \int_S \rho(x_1, x_2, x_3) \sum_{s=1}^3 v_s^2 d^3S \quad ; \quad (1b)$$

while the self potential-energy tensor and the self potential energy read (Chandrasekhar, 1969, Chap. 2, §10):

$$\begin{aligned} (E_{\text{sel}})_{pq} &= \int_S \rho(x_1, x_2, x_3) x_p \frac{\partial \mathcal{V}}{\partial x_q} d^3S \\ &= -\frac{1}{2} \int_S \rho(x_1, x_2, x_3) \mathcal{V}_{pq}(x_1, x_2, x_3) d^3S \quad ; \quad p = 1, 2, 3 \quad ; \quad q = 1, 2, 3 \quad ; \quad (2a) \end{aligned}$$

$$\begin{aligned} E_{\text{sel}} &= \int_S \rho(x_1, x_2, x_3) \sum_{s=1}^3 x_s \frac{\partial \mathcal{V}}{\partial x_s} d^3S \\ &= -\frac{1}{2} \int_S \rho(x_1, x_2, x_3) \mathcal{V}(x_1, x_2, x_3) d^3S \quad ; \quad (2b) \end{aligned}$$

where ρ is the density, $d^3S = dx_1 dx_2 dx_3$ an infinitesimal volume element placed at $\mathbf{P} = (x_1, x_2, x_3)$, $v_p v_q = \overline{v_p v_q}$ and $v_s^2 = \overline{(v_s^2)}$ are arithmetic means calculated within d^3S , \mathcal{V}_{pq} and \mathcal{V} are the gravitational tensor potential and potential, respectively (Chandrasekhar, 1969, Chap. 2, §10):

$$\mathcal{V}_{pq}(x_1, x_2, x_3) = G \int_S \rho(x'_1, x'_2, x'_3) \frac{(x'_p - x_p)(x'_q - x_q)}{|\vec{R} - \vec{R}'|^3} d^3S' ;$$

$$p = 1, 2, 3 ; \quad q = 1, 2, 3 ; \quad (3a)$$

$$\mathcal{V}(x_1, x_2, x_3) = G \int_S \rho(x'_1, x'_2, x'_3) \frac{d^3S'}{|\vec{R} - \vec{R}'|} ; \quad (3b)$$

G being the constant of gravitation, $\vec{R} = \overrightarrow{OP}$ and $\vec{R}' = \overrightarrow{OP'}$, $\mathbf{P}' = (x'_1, x'_2, x'_3)$, radius vectors with origin at the centre of inertia.

Conformly to Eq. (3), the normalization of the potential satisfies the boundary condition to be null at infinite distances, and then positive elsewhere (e.g., MacMillan, 1930, Chap. II, §20; Chandrasekhar, 1969, Chap. 3, §17; Caimmi and Secco, 2003), instead of being null at the centre of inertia, and then negative elsewhere (e.g., Binney and Tremaine, 1987, Chap. 2, §1; Mouri and Taniguchi, 2003).

Let i and j denote the subsystems of a two-component matter distribution. The potential-energy tensor and the potential energy may be cast into the form (Caimmi and Secco, 1992):

$$(E_{\text{pot}})_{pq} = [(E_i)_{\text{sel}}]_{pq} + [(E_{ij})_{\text{int}}]_{pq} + [(E_{ji})_{\text{int}}]_{pq} + [(E_j)_{\text{sel}}]_{pq} ; \quad (4a)$$

$$E_{\text{pot}} = (E_i)_{\text{sel}} + (E_{ij})_{\text{int}} + (E_{ji})_{\text{int}} + (E_j)_{\text{sel}} ; \quad (4b)$$

where the expression of the potential energy (e.g., MacMillan, 1930, Chap. III, §76) has been extended to the potential-energy tensor; in addition, the interaction potential-energy tensor, $[(E_{uv})_{\text{int}}]_{pq}$, and the interaction potential energy, $(E_{uv})_{\text{int}}$, read:

$$[(E_{uv})_{\text{int}}]_{pq} = -\frac{1}{2} \int_{S_u} \rho_u(x_1, x_2, x_3) [\mathcal{V}_v(x_1, x_2, x_3)]_{pq} d^3S ;$$

$$u = i, j ; \quad v = j, i ; \quad (5a)$$

$$(E_{uv})_{\text{int}} = -\frac{1}{2} \int_{S_u} \rho_u(x_1, x_2, x_3) \mathcal{V}_v(x_1, x_2, x_3) d^3S ;$$

$$u = i, j ; \quad v = j, i ; \quad (5b)$$

which are symmetric with respect to the exchange of one component with the other:

$$[(E_{ij})_{\text{int}}]_{pq} = [(E_{ji})_{\text{int}}]_{pq} ; \quad (6a)$$

$$(E_{ij})_{\text{int}} = (E_{ji})_{\text{int}} ; \quad (6b)$$

for further details refer to earlier attempts (MacMillan, 1930, Chap. III, §76; Caimmi and Secco, 1992).

The tidal potential-energy tensor and the tidal potential energy read (e.g., Caimmi and Secco, 1992):

$$[(E_{uv})_{\text{tid}}]_{pq} = \int_{S_u} \rho_u(x_1, x_2, x_3) x_p \frac{\partial \mathcal{V}_v}{\partial x_q} d^3 S \quad ;$$

$$u = i, j \quad ; \quad v = j, i \quad ; \quad (7a)$$

$$(E_{uv})_{\text{tid}} = \int_{S_u} \rho_u(x_1, x_2, x_3) \sum_{s=1}^3 x_s \frac{\partial \mathcal{V}_v}{\partial x_s} d^3 S \quad ;$$

$$u = i, j \quad ; \quad v = j, i \quad ; \quad (7b)$$

where the tidal potential energy, $(E_{uv})_{\text{tid}}$, may be conceived as the virial of the u -th component in connection with the tidal field induced by the v -th component (Brosche et al., 1983).

The tensor and the scalar virial theorem for a single subsystem, within the tidal field induced by the other one, read (Caimmi et al., 1984; Caimmi and Secco, 1992):

$$2[(E_u)_{\text{kin}}]_{pq} + [(E_u)_{\text{sel}}]_{pq} + [(E_{uv})_{\text{tid}}]_{pq} = 0 \quad ; \quad u = i, j \quad ; \quad v = j, i \quad ; \quad (8a)$$

$$2(E_u)_{\text{kin}} + (E_u)_{\text{sel}} + (E_{uv})_{\text{tid}} = 0 \quad ; \quad u = i, j \quad ; \quad v = j, i \quad ; \quad (8b)$$

which is the generalization of previous results related to one-component systems (e.g., Chandrasekhar, 1969, Chap. II, §11; Binney and Tremaine, 1987, Chap. 4, §3). The validity of the relations (Caimmi and Secco, 1992):

$$[(E_{ij})_{\text{tid}}]_{pq} + [(E_{ji})_{\text{tid}}]_{pq} = [(E_{ij})_{\text{int}}]_{pq} + [(E_{ji})_{\text{int}}]_{pq} \quad ; \quad (9a)$$

$$(E_{ij})_{\text{tid}} + (E_{ji})_{\text{tid}} = (E_{ij})_{\text{int}} + (E_{ji})_{\text{int}} \quad ; \quad (9b)$$

implies the following:

$$[(E_{uv})_{\text{tid}}]_{pq} = [(E_{uv})_{\text{int}}]_{pq} + [(E_{uv})_{\text{res}}]_{pq} \quad ; \quad u = i, j \quad ; \quad v = j, i \quad ; \quad (10a)$$

$$(E_{uv})_{\text{tid}} = (E_{uv})_{\text{int}} + (E_{uv})_{\text{res}} \quad ; \quad u = i, j \quad ; \quad v = j, i \quad ; \quad (10b)$$

where $[(E_{uv})_{\text{res}}]_{pq}$ and $(E_{uv})_{\text{res}}$ are the residual potential-energy tensor and the residual potential energy, respectively, which are antisymmetric with regard to the exchange of one component with the other:

$$[(E_{ij})_{\text{res}}]_{pq} = -[(E_{ji})_{\text{res}}]_{pq} \quad ; \quad (11a)$$

$$(E_{ij})_{\text{res}} = -(E_{ji})_{\text{res}} \quad ; \quad (11b)$$

for further details refer to earlier attempts (Caimmi and Secco, 1992; Caimmi, 2007b).

It can be seen from Eqs. (6), (10), and (11), that the tidal potential-energy tensor, $[(E_{uv})_{\text{tid}}]_{pq}$, and the tidal potential energy, $(E_{uv})_{\text{tid}}$, are made of a symmetric term, $[(E_{uv})_{\text{int}}]_{pq}$ and $(E_{uv})_{\text{int}}$, and an antisymmetric term, $[(E_{uv})_{\text{res}}]_{pq}$ and $(E_{uv})_{\text{res}}$, respectively, with regard to the exchange of one component with the other.

The virial theorem in tensor and in scalar form, expressed by Eqs. (8), may be cast into the more compact form:

$$2[(E_u)_{\text{kin}}]_{pq} + [(E_{uv})_{\text{vir}}]_{pq} = 0 \quad ; \quad u = i, j \quad ; \quad v = j, i \quad ; \quad (12a)$$

$$2(E_u)_{\text{kin}} + (E_{uv})_{\text{vir}} = 0 \quad ; \quad u = i, j \quad ; \quad v = j, i \quad ; \quad (12b)$$

where the virial potential-energy tensor, $[(E_{uv})_{\text{vir}}]_{pq}$, and the virial potential energy, $(E_{uv})_{\text{vir}}$, are defined as:

$$[(E_{uv})_{\text{vir}}]_{pq} = [(E_u)_{\text{sel}}]_{pq} + [(E_{uv})_{\text{tid}}]_{pq} \quad ; \quad u = i, j \quad ; \quad v = j, i \quad ; \quad (13a)$$

$$(E_{uv})_{\text{vir}} = (E_u)_{\text{sel}} + (E_{uv})_{\text{tid}} \quad ; \quad u = i, j \quad ; \quad v = j, i \quad ; \quad (13b)$$

where, in general, the virial potential energy is usually named “the virial of the system” (Clausius, 1870). In the case under discussion, the “system” relates to the u -th component within the tidal potential induced by the v -th component.

For assigned density profiles, the virial potential-energy tensor and the virial energy of each subsystem can be determined, together with their kinetic counterparts via Eqs. (12a) and (12b), respectively, which constrain, in turn, the orbital anisotropy on each subsystem. More specifically, the sum of mean orbital kinetic-energy tensor and kinetic energy, has to reproduce $[(E_u)_{\text{kin}}]_{pq}$ and $(E_u)_{\text{kin}}$, respectively.

When a system is not entirely included within its truncation radius, the usual form of the virial theorem, $2E_{\text{kin}} + E_{\text{pot}} = 0$, should be extended as $2E_{\text{kin}} + E_{\text{pot}} = 3pS$, where the last is a surface term (e.g., The and White, 1986; Carlberg et al., 1996; Girardi et al., 1998). In dealing with a specified subsystem, it shall be intended that no mass exists outside the related truncation radius, which makes a null surface term.

To avoid the determination of the gravitational potential, which is the most difficult step towards an explicit expression of the potential-energy tensors and potential energies, a particular procedure shall be followed under the restrictive assumption of homeoidally striated density profiles (Roberts, 1962).

2.2 Homeoidally striated density profiles

Let the isopycnic (i.e. constant density) surfaces be defined by the following law (CM03):

$$\rho = \rho^\dagger f(\xi) \quad ; \quad f(1) = 1 \quad ; \quad (14a)$$

$$\xi^2 = \sum_{\ell=1}^3 \frac{x_\ell^2}{(a_\ell^\dagger)^2} \quad ; \quad 0 \leq \xi \leq \Xi \quad ; \quad (14b)$$

where $\rho^\dagger = \rho(1)$, a_ℓ^\dagger , are the density and the semiaxes, respectively, of a reference isopycnic surface, and Ξ corresponds to the truncation isopycnic surface, related to semiaxes, a_ℓ . The scaled radial coordinate, ξ , and the scaled density, f , may be conceived as the generalization of their counterparts related to polytropes (e.g., Chandrasekhar, 1939, Chap. IV, §4; Horedt, 2004, Chap. 2, §2.1).

According to Eqs. (14), the scaling density, ρ^\dagger , and the scaling radius, r^\dagger , correspond to a single boundary, which allows the description of both cored and cuspy density profiles. The assumption that the system is homeoidally striated implies the relation (CM03):

$$\xi = \frac{r}{r^\dagger} \quad ; \quad (15)$$

and, in particular:

$$\Xi = \frac{R}{r^\dagger} \quad ; \quad (16)$$

which, in any case, is independent of the radial coordinate, r , of the generic point on the selected isopycnic surface.

2.3 Mass and inertia tensor

The function (Roberts, 1962):

$$F(\xi) = 2 \int_\xi^\Xi f(\xi') \xi' d\xi' \quad ; \quad (17a)$$

$$F(\Xi) = 0 \quad ; \quad \frac{dF}{d\xi} = -2\xi f(\xi) \quad ; \quad (17b)$$

$$\int_0^\Xi f(\xi) \xi^n d\xi = \frac{n-1}{2} \int_0^\Xi F(\xi) \xi^{n-2} d\xi \quad ; \quad n > 1 \quad ; \quad (17c)$$

allows the calculation of the total mass as (CM03):

$$M = \nu_{\text{mas}} M^\dagger \quad ; \quad (18a)$$

$$\nu_{\text{mas}} = \frac{3}{2} \int_0^\Xi F(\xi) d\xi ; \quad (18b)$$

$$M^\dagger = \frac{4\pi}{3} \rho^\dagger a_1^\dagger a_2^\dagger a_3^\dagger ; \quad (18c)$$

and the inertia tensor as (CM03):

$$I_{pq} = \delta_{pq} \nu_{\text{inr}} M^\dagger (a_p^\dagger)^2 ; \quad (19a)$$

$$\nu_{\text{inr}} = \frac{3}{2} \int_0^\Xi F(\xi) \xi^2 d\xi ; \quad (19b)$$

where the coefficients, ν_{mas} and ν_{inr} , are shape-independent and may be conceived as profile factors (Caimmi, 1993), and δ_{pq} is the Kronecker symbol. For a different formulation of the inertia tensor refer to earlier attempts (e.g., Landau and Lifchitz, 1966, Chap. VI, §32; Bett et al., 2007).

The mass within an isopycnic surface, $\rho = \rho^\dagger f(\xi)$, is $M(\xi) = \nu_{\text{mas}}(\xi) M^\dagger$, where $\nu_{\text{mas}}(\xi)$ is expressed by Eq. (18b) with ξ instead of Ξ . The related mean density is $\bar{\rho}(\xi) = M(\xi)/S(\xi)$, where $S(\xi)$ is the volume bounded by the isopycnic surface.

2.4 Potential-energy tensors and potential energies

The self potential-energy tensor and the self potential energy read (CM03):

$$(E_{\text{sel}})_{pq} = -\delta_{pq} \nu_{\text{sel}} \frac{G(M^\dagger)^2}{a_1^\dagger} B_p ; \quad (20a)$$

$$E_{\text{sel}} = -\nu_{\text{sel}} \frac{G(M^\dagger)^2}{a_1^\dagger} B ; \quad (20b)$$

$$\nu_{\text{sel}} = \frac{9}{16} \int_0^\Xi F^2(\xi) d\xi ; \quad (20c)$$

$$B_p = \epsilon_{p2} \epsilon_{p3} \int_0^{+\infty} (1+s')^{-3/2} (1+\epsilon_{pq}^2 s')^{-1/2} (1+\epsilon_{pr}^2 s')^{-1/2} ds' ; \quad (20d)$$

$$B = \sum_{s=1}^3 B_p ; \quad \epsilon_{mn} = \frac{a_m}{a_n} ; \quad (20e)$$

where ν_{sel} is a profile factor, ϵ_{mn} are axis ratios, and B_p are profile factors which, *ipso facto*, depend on the axis ratios only (Caimmi, 1992).

The above results are related to a single subsystem: strictly speaking, all the quantities defined in the current section should be labelled by the index, u , in connection with the u -th subsystem (e.g., Caimmi and Secco, 1992), but it has been omitted to gain clarity. On the other hand, the formulation of other potential-energy tensors and potential energies necessarily involves

(at least) two components. The related calculations are very difficult in the general case, and for this reason only the special situation of similar and similarly placed boundaries shall be considered.

With this restriction, the combination of Eqs. (15), (16), and (18c), related to both the density profiles, the inner to be denoted as i and the outer as j , yields:

$$\xi_i = y^\dagger \xi_j \quad ; \quad \frac{\Xi_j}{\Xi_i} = \frac{y}{y^\dagger} \quad ; \quad \frac{(\nu_j)_{\text{mas}}}{(\nu_i)_{\text{mas}}} = \frac{m}{m^\dagger} \quad ; \quad (21a)$$

$$y = \frac{R_j}{R_i} \quad ; \quad y^\dagger = \frac{r_j^\dagger}{r_i^\dagger} \quad ; \quad m = \frac{M_j}{M_i} \quad ; \quad m^\dagger = \frac{M_j^\dagger}{M_i^\dagger} \quad ; \quad (21b)$$

which allows the expression of the other potential-energy tensors and potential energies, as (CM03):

$$[(E_{uv})_{\text{xxx}}]_{pq} = -\delta_{pq} \frac{G(M_u^\dagger)^2}{(a_u^\dagger)_1} (\nu_{uv})_{\text{xxx}} B_p \quad ; \quad (22a)$$

$$(E_{uv})_{\text{xxx}} = -\frac{G(M_u^\dagger)^2}{(a_u^\dagger)_1} (\nu_{uv})_{\text{xxx}} B \quad ; \quad (22b)$$

$$u = i, j \quad ; \quad v = j, i \quad ; \quad \text{xxx} = \text{int, tid, res, vir} \quad ; \quad (22c)$$

and the explicit expression of the profile factors reads (CM03):

$$(\nu_{ij})_{\text{int}} = (\nu_{ji})_{\text{int}} = -\frac{9}{16} m^\dagger \left[w^{(\text{int})}(\eta) + w^{(\text{ext})}(\eta) \right] \quad ; \quad (23a)$$

$$(\nu_{ij})_{\text{tid}} = -\frac{9}{8} m^\dagger w^{(\text{ext})}(\eta) \quad ; \quad (\nu_{ji})_{\text{tid}} = -\frac{9}{8} \frac{y^\dagger}{m^\dagger} w^{(\text{int})}(\eta) \quad ; \quad (23b)$$

$$(\nu_{ij})_{\text{res}} = -(\nu_{ji})_{\text{res}} = -\frac{9}{16} m^\dagger \left[w^{(\text{int})}(\eta) - w^{(\text{ext})}(\eta) \right] \quad ; \quad (23c)$$

$$(\nu_{uv})_{\text{vir}} = (\nu_u)_{\text{sel}} + (\nu_{uv})_{\text{tid}} \quad ; \quad u = i, j \quad ; \quad v = j, i \quad ; \quad (23d)$$

$$\eta = \frac{\Xi_i}{y^\dagger} = \frac{\Xi_j}{y} \quad ; \quad (23e)$$

where the functions, $w^{(\text{int})}$ and $w^{(\text{ext})}$, are defined as (CM03):

$$w^{(\text{int})}(\eta) = \int_0^\eta F_j(\xi_j) \frac{dF_i}{d\xi_j} \xi_j d\xi_j \quad ; \quad (24a)$$

$$w^{(\text{ext})}(\eta) = \int_0^\eta F_i(\xi_i) \frac{dF_j}{d\xi_j} \xi_j d\xi_j \quad ; \quad (24b)$$

in conclusion, Eqs. (20)-(24) allow the calculation of the potential-energy tensors and potential energies for homeoidally striated density profiles related to similar and similarly placed boundaries.

In the case under discussion, due to Eqs. (22), the fractional virial potential-energy tensor component equals the fractional virial potential energy, as:

$$\phi = \frac{[(E_{ji})_{\text{vir}}]_{pq}}{[(E_{ij})_{\text{vir}}]_{pq}} = \frac{(E_{ji})_{\text{vir}}}{(E_{ij})_{\text{vir}}} = \frac{(m^\dagger)^2 (\nu_{ji})_{\text{vir}}}{y^\dagger (\nu_{ij})_{\text{vir}}} ; \quad (25)$$

which, for assigned density profiles, depends on the reference fractional mass, m^\dagger , and the fractional scaling radius, y^\dagger , according to Eqs. (21)-(24). The substitution of Eqs. (21) into (25) yields:

$$\phi = \frac{m^2}{y} \frac{\Xi_j}{\Xi_i} \left[\frac{(\nu_i)_{\text{mas}}}{(\nu_j)_{\text{mas}}} \right]^2 \frac{(\nu_{ji})_{\text{vir}}}{(\nu_{ij})_{\text{vir}}} ; \quad (26)$$

which, for assigned density profiles, depends on the fractional mass, m , and the fractional truncation radius, y , according to Eqs. (21)-(24).

Strictly speaking, Eqs. (21)-(26) are valid provided the indices, i and j , denote the embedded and the embedding subsystem, respectively, which implies $y \geq 1$. This is why the above procedure is valid only for the inner component, where the Poisson equation instead of the Laplace equation holds with respect to the gravitational potential. The remaining results, related to the outer component, are obtained by use of the symmetry of the interaction potential-energy tensor and interaction potential energy, Eqs. (6), and the antisymmetry of the residual potential-energy tensor and residual potential energy, Eqs. (11).

If the role of the two subsystems is reversed, $0 \leq y \leq 1$, it has to be kept in mind that, in this case, the inner and the outer component are denoted by the indices, j and i , respectively, and the reversion must be done in Eqs. (21)-(26), through the following steps: (i) make the changes: $m \rightarrow m^{-1}$; $m^\dagger \rightarrow (m^\dagger)^{-1}$; $y \rightarrow y^{-1}$; $y^\dagger \rightarrow (y^\dagger)^{-1}$; $\Xi_i \leftrightarrow \Xi_j$; $(\nu_i)_{\text{mas}} \leftrightarrow (\nu_j)_{\text{mas}}$; $(\nu_i)_{\text{sel}} \leftrightarrow (\nu_j)_{\text{sel}}$; (ii) for assigned $y \geq 1$ and $y^\dagger = (\Xi_i/\Xi_j)y$, calculate the functions, $w^{(\text{int})}(\eta)$ and $w^{(\text{ext})}(\eta)$; (iii) calculate the profile factors, $(\nu_{ij})_{\text{tid}}$ and $(\nu_{ji})_{\text{tid}}$, and the remaining ones when needed; (iv) calculate the fractional virial potential energy, ϕ ; (v) make the changes, $m \rightarrow m^{-1}$; $m^\dagger \rightarrow (m^\dagger)^{-1}$; $y \rightarrow y^{-1}$; $y^\dagger \rightarrow (y^\dagger)^{-1}$; $\phi \rightarrow \phi^{-1}$; which allow the extension of the fractional virial potential energy, $\phi = (E_{ji})_{\text{vir}}/(E_{ij})_{\text{vir}}$, to the domain, $0 \leq y \leq 1$.

In absence of truncation radius, $\Xi \rightarrow +\infty$, $\eta \rightarrow +\infty$, the reversion occurs when the density drops to zero and nothing changes except in infinitesimal terms of higher order and infinite terms of lower order. Accordingly, there is no need to perform the reversion in this case.

The relation, $\phi = \phi(y^\dagger, m^\dagger)$, or its counterpart, $\phi = \phi(y, m)$, expressed by Eqs. (25) and (26), respectively, may be conceived as an equation of state for two-component systems with assigned homeoidally striated density profiles.

At the price of a major complexity, it can be formulated for any kind of two-component systems, hereafter quoted as “two-component macrogases”, or more shortly as “macrogases”.

3 Special cases

The explicit expression of the macrogases equation of state is, in general, rather cumbersome and numerical computations should be preferred to this aim. On the other hand, the related procedure is conceptually simple, as the functions, $w^{(\text{int})}(\eta)$ and $w^{(\text{ext})}(\eta)$, and the fractional virial potential energy, ϕ , may be calculated using Eqs. (20)-(26).

Aiming to provide a description of the general trend and related features, a limited number of simple possibilities shall be analysed in detail, selecting density profiles from the family:

$$f(\xi) = \frac{2^\chi}{\xi^\gamma(1 + \xi^\alpha)^\chi} \quad ; \quad \chi = \frac{\beta - \gamma}{\alpha} \quad ; \quad (27)$$

which is defined by three parameters, (α, β, γ) . For further details refer to earlier attempts (e.g., Hernquist, 1990; Zhao, 1996; Caimmi and Marmo, 2004; Caimmi et al., 2005; Caimmi, 2006b), where special cases were fully investigated.

In the following, the macrogases equation of state shall be determined for a simple but unrealistic density profile, to be taken as a reference case, and a few density profiles of astrophysical interest. The reader whose attention is mainly directed to the results and/or the astrophysical applications of the model, is free to jump directly to Section 4 and/or 5, respectively.

3.1 UU macrogases

The related density profiles maintain uniform, $(\alpha, \beta, \gamma) = (0, 0, 0)$, and Eq. (27) reduces to:

$$f_u(\xi_u) = 1 \quad ; \quad 0 \leq \xi_u \leq \Xi_u \quad ; \quad u = i, j \quad ; \quad (28)$$

which is equivalent to polytropes with index, $n = 0$ (e.g., Chandrasekhar, 1939, Chap. IV, §4; Caimmi, 1986) but implies unphysical situations for stellar fluids (Vandervoort, 1980). The particularization of Eqs. (17a), (18b), (20c), (24a), and (24b) to the case of interest yields:

$$F_u(\xi_u) = \Xi_u^2 - \xi_u^2 \quad ; \quad u = i, j \quad ; \quad (29)$$

$$(\nu_u)_{\text{mas}} = \Xi_u^3 ; \quad u = i, j ; \quad (30)$$

$$(\nu_u)_{\text{sel}} = \frac{3}{10} \Xi_u^5 ; \quad u = i, j ; \quad (31)$$

$$w^{(\text{int})}(\eta) = -\frac{4}{15} \Xi_i^2 \eta^3 \left(\frac{5}{2} y^2 - \frac{3}{2} \right) ; \quad (32)$$

$$w^{(\text{ext})}(\eta) = -\frac{4}{15} \Xi_i^2 \eta^3 ; \quad (33)$$

and, using Eqs. (23b) and (23e), the UU macrogases equation of state follows from the particularization of Eq. (26) to the case of interest, as:

$$\phi = \frac{(m^\dagger)^2}{y^\dagger} \left(\frac{y}{y^\dagger} \right)^5 \frac{1 + \frac{(y^\dagger)^3}{(m^\dagger)} \frac{1}{y^5} \left(\frac{5}{2} y^2 - \frac{3}{2} \right)}{1 + \frac{m^\dagger}{(y^\dagger)^3}} ; \quad y \geq 1 ; \quad (34)$$

and the extension of the above function to the domain, $0 \leq y \leq 1$, following the procedure outlined in Subsection 2.4, yields:

$$\phi = \left(\frac{y}{y^\dagger} \right)^5 \frac{m^\dagger (y^\dagger)^2 \left[1 + \frac{m^\dagger}{(y^\dagger)^3} \right]}{1 + m^\dagger \left(\frac{y}{y^\dagger} \right)^3 \left(\frac{5}{2} - \frac{3}{2} y^2 \right)} ; \quad 0 \leq y \leq 1 ; \quad (35)$$

where it can be seen that in the special case, $y = 1$, Eqs. (34) and (35) do coincide. If, in addition, $\Xi_i = \Xi_j$, which implies $y^\dagger = y$, $m^\dagger = m$, via Eqs. (18) and (21), then Eqs. (34) and (35) reduce to:

$$\phi = m = m^\dagger ; \quad y = y^\dagger = 1 ; \quad (36)$$

or $\phi(1, m) = m$.

Owing to Eqs. (34) and (35), the fractional virial potential energy, ϕ , is independent of the fractional truncation radii, (Ξ_i, Ξ_j) .

3.2 PP macrogases

The related density profiles (Schuster, 1883; Plummer, 1911) imply $(\alpha, \beta, \gamma) = (2, 5, 0)$, and Eq. (27) reduces to:

$$f_u(\xi_u) = \frac{2^{5/2}}{(1 + \xi_u^2)^{5/2}} ; \quad 0 \leq \xi_u \leq \Xi_u ; \quad u = i, j ; \quad (37)$$

which is equivalent to polytropes with index, $n = 5$; for a formal demonstration, see Appendix A. For one-component systems, hydrostatic equilibrium holds regardless from the nature of the fluid (Vandervoort, 1980).

The particularization of Eqs. (17a), (18b), (20c), (24a), and (24b) to the case of interest yields:

$$F_u(\xi_u) = \frac{2^{7/2}}{3} \left[\frac{1}{(1 + \xi_u^2)^{3/2}} - \frac{1}{(1 + \Xi_u^2)^{3/2}} \right] ; \quad u = i, j ; \quad (38)$$

$$(\nu_u)_{\text{mas}} = \frac{2^{5/2} \Xi_u^3}{(1 + \Xi_u^2)^{3/2}} ; \quad u = i, j ; \quad (39)$$

$$(\nu_u)_{\text{sel}} = \frac{\Xi_u(3\Xi_u^4 - 8\Xi_u^2 + 13)}{(1 + \Xi_u^2)^3} + 3 \arctan \Xi_u ; \quad u = i, j ; \quad (40)$$

$$w^{(\text{int})}(\eta) = -\frac{128}{3}(y^\dagger)^2 \left\{ \frac{[(y^\dagger)^2 + 7]iE(y^\dagger, i\alpha) + 4[(y^\dagger)^2 - 1]iF(y^\dagger, i\alpha)}{3[(y^\dagger)^2 - 1]^3} \right. \\ \left. + \frac{P^{(\text{int})}(\eta, y^\dagger)}{3[(y^\dagger)^2 - 1]^3(\eta^2 + 1)[(y^\dagger)^2\eta^2 + 1]^2} - \frac{1}{(1 + \Xi_j^2)^{3/2}} \frac{\eta^3}{3[(y^\dagger)^2\eta^2 + 1]^{3/2}} \right\} ; \quad (41a)$$

$$P^{(\text{int})}(\eta, y^\dagger) = \eta\sqrt{\eta^2 + 1}\sqrt{(y^\dagger)^2\eta^2 + 1} \\ \times [(y^\dagger)^6\eta^2(\eta^2 + 1) + (y^\dagger)^4\eta^2(7\eta^2 - 4) + (y^\dagger)^2(11\eta^2 + 5) + 3] ; \quad (41b)$$

$$\alpha = \text{arcsinh } \eta ; \quad y^\dagger \neq 1 ; \quad (41c)$$

$$w^{(\text{int})}(\eta) = -\frac{128}{3}(y^\dagger)^2 \left[\frac{\arctan \eta}{16} + \frac{\eta(3\eta^4 + 8\eta^2 - 3)}{48(\eta^2 + 1)^3} \right. \\ \left. - \frac{1}{(1 + \Xi_j^2)^{3/2}} \frac{\eta^3}{3(\eta^2 + 1)^{3/2}} \right] ; \quad y^\dagger = 1 ; \quad (41d)$$

$$w^{(\text{ext})}(\eta) = -\frac{128}{3} \left\{ -\frac{[7(y^\dagger)^2 + 1]iE(y^\dagger, i\alpha) + [3(y^\dagger)^4 - 2(y^\dagger)^2 - 1]iF(y^\dagger, i\alpha)}{3[(y^\dagger)^2 - 1]^3} \right. \\ \left. - \frac{P^{(\text{ext})}(\eta, y^\dagger)}{3[(y^\dagger)^2 - 1]^3(\eta^2 + 1)^2[(y^\dagger)^2\eta^2 + 1]} - \frac{1}{(1 + \Xi_i^2)^{3/2}} \frac{\eta^3}{3(\eta^2 + 1)^{3/2}} \right\} ; \quad (42a)$$

$$P^{(\text{ext})}(\eta, y^\dagger) = \eta\sqrt{\eta^2 + 1}\sqrt{(y^\dagger)^2\eta^2 + 1} \\ \times [(y^\dagger)^4(7\eta^4 + 11\eta^2 + 3) + (y^\dagger)^2(\eta^4 + 4\eta^2 + 5) + \eta^2] ; \quad (42b)$$

$$\alpha = \text{arcsinh } \eta ; \quad y^\dagger \neq 1 ; \quad (42c)$$

$$w^{(\text{ext})}(\eta) = -\frac{128}{3} \left[\frac{\arctan \eta}{16} + \frac{\eta(3\eta^4 + 8\eta^2 - 3)}{48(\eta^2 + 1)^3} \right. \\ \left. - \frac{1}{(1 + \Xi_i^2)^{3/2}} \frac{\eta^3}{3(\eta^2 + 1)^{3/2}} \right] ; \quad y^\dagger = 1 ; \quad (42d)$$

where i is the imaginary unit, F and E are incomplete elliptic integrals of the first and second kind, respectively, defined as:

$$F(k, \beta) = \int_0^\beta \frac{d\theta}{\sqrt{1 - k^2 \sin^2 \theta}} = \int_0^x \frac{dt}{\sqrt{1 - t^2} \sqrt{1 - k^2 t^2}} ; \quad (43a)$$

$$E(k, \beta) = \int_0^\beta \sqrt{1 - k^2 \sin^2 \theta} d\theta = \int_0^x \frac{\sqrt{1 - k^2 t^2}}{\sqrt{1 - t^2}} dt ; \quad (43b)$$

$$x = \sin \beta ; \quad t = \sin \theta ; \quad (43c)$$

for further details refer to specialized textbooks (e.g., Spiegel, 1968, Chap. 4, §§34.1-4).

Using Eqs. (23b) and (39)-(42), the PP macrogases equation of state is obtained from the particularization of Eq. (26) to the case of interest for the domain, $y \geq 1$. The extension to the domain, $0 \leq y \leq 1$, can be done following the procedure outlined in Subsection 2.4.

In absence of truncation radius, the density drops to zero when the radius goes to infinity, $\Xi \rightarrow +\infty$, $\eta \rightarrow +\infty$, and Eqs. (38)-(42) reduce to:

$$\lim_{\Xi_u \rightarrow +\infty} F_u(\xi_u) = \frac{2^{7/2}}{3} \frac{1}{(1 + \xi_u^2)^{3/2}} ; \quad u = i, j ; \quad (44)$$

$$\lim_{\Xi_u \rightarrow +\infty} (\nu_u)_{\text{mas}} = 2^{5/2} ; \quad u = i, j ; \quad (45)$$

$$\lim_{\Xi_u \rightarrow +\infty} (\nu_u)_{\text{sel}} = \frac{3\pi}{2} ; \quad u = i, j ; \quad (46)$$

$$\lim_{\eta \rightarrow +\infty} w^{(\text{int})}(\eta) = -\frac{128}{3} (y^\dagger)^2 \frac{[(y^\dagger)^2 + 7]E(k, \pi/2) - [5(y^\dagger)^2 + 3]F(k, \pi/2)}{3[(y^\dagger)^2 - 1]^3} ;$$

$$k = \sqrt{1 - (y^\dagger)^2} ; \quad y^\dagger \neq 1 ; \quad (47a)$$

$$\lim_{\eta \rightarrow +\infty} w^{(\text{int})}(\eta) = -\frac{4\pi}{3} ; \quad y^\dagger = 1 ; \quad (47b)$$

$$\lim_{\eta \rightarrow +\infty} w^{(\text{ext})}(\eta) = -\frac{128}{3} y^\dagger \frac{[3(y^\dagger)^2 + 5]F(k, \pi/2) - [7(y^\dagger)^2 + 1]E(k, \pi/2)}{3[(y^\dagger)^2 - 1]^3} ;$$

$$k = \sqrt{1 - 1/(y^\dagger)^2} ; \quad y^\dagger \neq 1 ; \quad (48a)$$

$$\lim_{\eta \rightarrow +\infty} w^{(\text{ext})}(\eta) = -\frac{4\pi}{3} ; \quad y^\dagger = 1 ; \quad (48b)$$

where, in particular, the related expression of the tidal energy coincides with its counterpart calculated in an earlier attempt (Valentinuzzi, 2006, Chap. 4,

§4.1). Using Eqs. (23b) and (45)-(48), the PP macrogases equation of state in the special situation under discussion, is obtained from the particularization of Eq. (26) to the case of interest, for the domain, $y \geq 0$.

If, in addition, $y = y^\dagger = 1$, $\Xi_j = \Xi_i$, the combination of Eqs. (26) and (45)-(48) yields Eq. (36).

3.3 HH macrogases

The related density profiles (Hernquist, 1990) imply $(\alpha, \beta, \gamma) = (1, 4, 1)$, and Eq. (27) reduces to:

$$f_u(\xi_u) = \frac{8}{\xi_u(1 + \xi_u)^3} ; \quad 0 \leq \xi_u \leq \Xi_u ; \quad u = i, j ; \quad (49)$$

which has been proved to be consistent with nonnegative distribution functions, in the parameter range of interest (Ciotti, 1996).

The particularization of Eqs. (17a), (18b), (20c), (24a), and (24b) to the case of interest yields:

$$F_u(\xi_u) = \frac{8}{(1 + \xi_u)^2} - \frac{8}{(1 + \Xi_u)^2} ; \quad u = i, j ; \quad (50)$$

$$(\nu_u)_{\text{mas}} = \frac{12\Xi_u^2}{(1 + \Xi_u)^2} ; \quad u = i, j ; \quad (51)$$

$$(\nu_u)_{\text{sel}} = \frac{12\Xi_u^3(4 + \Xi_u)}{(1 + \Xi_u)^4} ; \quad u = i, j ; \quad (52)$$

$$\begin{aligned} w^{(\text{int})}(\eta) = & -128y^\dagger \left\{ \frac{1}{2} \frac{1}{(y^\dagger - 1)^4} \left[-\frac{(y^\dagger - 1)^2 y^\dagger \eta}{(y^\dagger \eta + 1)^2} + \frac{2(y^\dagger - 1)\eta}{1 + \eta} \right. \right. \\ & + \frac{(y^\dagger - 1)(y^\dagger + 3)y^\dagger \eta}{y^\dagger \eta + 1} + 2(2y^\dagger + 1) \ln \frac{\eta + 1}{y^\dagger \eta + 1} \left. \right] \\ & - \frac{1}{2} \frac{1}{(1 + \Xi_j)^2} \frac{1}{(y^\dagger)^2} \left[1 - \frac{2y^\dagger \eta + 1}{(y^\dagger \eta + 1)^2} \right] \left. \right\} ; \quad y^\dagger \neq 1 ; \quad (53a) \end{aligned}$$

$$\begin{aligned} w^{(\text{int})}(\eta) = & -128 \left\{ \frac{1}{12} \left[-\frac{4\eta + 1}{(\eta + 1)^4} + 1 \right] \right. \\ & \left. - \frac{1}{2} \frac{1}{(1 + \Xi_j)^2} \frac{\eta^2}{(\eta + 1)^2} \right\} ; \quad y^\dagger = 1 ; \quad (53b) \end{aligned}$$

$$w^{(\text{ext})}(\eta) = -128 \left\{ -\frac{1}{2} \frac{1}{(y^\dagger - 1)^4} \left[\frac{(y^\dagger - 1)^2 \eta}{(\eta + 1)^2} + \frac{2(y^\dagger)^2 (y^\dagger - 1)\eta}{1 + y^\dagger \eta} \right] \right.$$

$$+\frac{(y^\dagger-1)(3y^\dagger+1)\eta}{\eta+1}-2y^\dagger(y^\dagger+2)\ln\frac{y^\dagger\eta+1}{\eta+1}\Bigg] \\ -\frac{1}{2}\frac{1}{(1+\Xi_i)^2}\frac{\eta^2}{(\eta+1)^2}\Bigg\} \quad ; \quad y^\dagger \neq 1 \quad ; \quad (54a)$$

$$w^{(\text{ext})}(\eta) = 128 \left\{ \frac{1}{12} \left[\frac{4\eta+1}{(\eta+1)^4} - 1 \right] \right. \\ \left. + \frac{1}{2} \frac{1}{(1+\Xi_i)^2} \frac{\eta^2}{(\eta+1)^2} \right\} \quad ; \quad y^\dagger = 1 \quad ; \quad (54b)$$

using Eqs. (23b) and (51)-(54), the HH macrogases equation of state is obtained from the particularization of Eq. (26) to the case of interest for the domain, $y \geq 1$. The extension to the domain, $0 \leq y \leq 1$, can be done following the procedure outlined in Subsection 2.4.

In absence of truncation radius, the density drops to zero when the radius goes to infinity, $\Xi \rightarrow +\infty$, $\eta \rightarrow +\infty$, and Eqs. (50)-(54) reduce to:

$$\lim_{\Xi_u \rightarrow +\infty} F_u(\xi_u) = \frac{8}{(1+\xi_u)^2} \quad ; \quad u = i, j \quad ; \quad (55)$$

$$\lim_{\Xi_u \rightarrow +\infty} (\nu_u)_{\text{mas}} = 12 \quad ; \quad u = i, j \quad ; \quad (56)$$

$$\lim_{\Xi_u \rightarrow +\infty} (\nu_u)_{\text{sel}} = 12 \quad ; \quad u = i, j \quad ; \quad (57)$$

$$\lim_{\eta \rightarrow +\infty} w^{(\text{int})}(\eta) = -\frac{64y^\dagger}{(y^\dagger-1)^4} \left[-2(2y^\dagger+1)\ln y^\dagger + (y^\dagger-1)(y^\dagger+5) \right] \quad ; \\ y^\dagger \neq 1 \quad ; \quad (58a)$$

$$\lim_{\eta \rightarrow +\infty} w^{(\text{int})}(\eta) = -\frac{32}{3} \quad ; \quad y^\dagger = 1 \quad ; \quad (58b)$$

$$\lim_{\eta \rightarrow +\infty} w^{(\text{ext})}(\eta) = -\frac{64}{(y^\dagger-1)^4} \left[2y^\dagger(y^\dagger+2)\ln y^\dagger - (y^\dagger-1)(5y^\dagger+1) \right] \quad ; \\ y^\dagger \neq 1 \quad ; \quad (59a)$$

$$\lim_{\eta \rightarrow +\infty} w^{(\text{ext})}(\eta) = -\frac{32}{3} \quad ; \quad y^\dagger = 1 \quad ; \quad (59b)$$

where, in particular, the related expression of the tidal energy coincides with its counterpart calculated in an earlier attempt (Valentinuzzi, 2006, Chap. 4, §4.2.1). Using Eqs. (23b) and (56)-(59), the HH macrogases equation of state in the special situation under discussion, is obtained from the particularization of Eq. (26) to the case of interest, for the domain, $y \geq 0$. If, in particular, $y = y^\dagger = 1$, $\Xi_j = \Xi_i$, the combination of Eqs. (26) and (56)-(59) yields Eq. (36).

3.4 HP macrogases

The inner density profile (Hernquist, 1990) implies $(\alpha, \beta, \gamma) = (1, 4, 1)$, which is defined by Eq. (49), and related functions and parameters by Eqs. (50)-(52) or (55)-(57) in the special case of no truncation radius.

The outer density profile (Schuster, 1883; Plummer, 1911) implies $(\alpha, \beta, \gamma) = (2, 5, 0)$, which is defined by Eq. (37), and related functions and parameters by Eqs. (38)-(40) or (44)-(46) in the special case of no truncation radius.

With regard to the tidal potential-energy terms, the particularization of Eqs. (24a) and (24b) to the case of interest yields:

$$w^{(\text{int})}(\eta) = -\frac{128\sqrt{2}}{3}y^\dagger \left[\Phi_1^{(\text{int})}(\eta) + \Phi_2^{(\text{int})}(\eta) - \frac{1}{2} \frac{\eta^2}{(1 + \Xi_j)^{3/2}} \right] ; \quad (60a)$$

$$\Phi_1^{(\text{int})}(\eta) = \frac{(y^\dagger)^4 - 12(y^\dagger)^2 + 2}{2[(y^\dagger)^2 + 1]^3} + \frac{P^{(\text{int})}(\eta)}{2[(y^\dagger)^2 + 1]^3(y^\dagger\eta + 1)^2(\eta^2 + 1)^{1/2}} ; \quad (60b)$$

$$\Phi_2^{(\text{int})}(\eta) = -\frac{3y^\dagger[3(y^\dagger)^2 - 2]}{2[(y^\dagger)^2 + 1]^{7/2}} \ln \frac{[y^\dagger - \eta + \sqrt{(y^\dagger)^2 + 1}\sqrt{\eta^2 + 1}]}{(y^\dagger\eta + 1)[y^\dagger + \sqrt{(y^\dagger)^2 + 1}]} ; \quad (60c)$$

$$P^{(\text{int})}(\eta) = -2(y^\dagger)^5\eta(2\eta^2 + 1) + (y^\dagger)^4(\eta^2 - 1) + (y^\dagger)^3\eta(11\eta^2 + 15) + 4(y^\dagger)^2(4\eta^2 + 3) + 2y^\dagger\eta - 2 ; \quad (60d)$$

$$w^{(\text{ext})}(\eta) = -64\sqrt{2} \left[\Phi_1^{(\text{ext})}(\eta) + \Phi_2^{(\text{ext})}(\eta) - \frac{1}{3} \frac{1}{(1 + \Xi_i)^2} \frac{\eta^3}{(1 + \eta^2)^{3/2}} \right] ; \quad (61a)$$

$$\Phi_1^{(\text{ext})}(\eta) = \frac{11(y^\dagger)^3 - 4y^\dagger}{3[(y^\dagger)^2 + 1]^3} + \frac{P^{(\text{ext})}(\eta)}{3[(y^\dagger)^2 + 1]^3(y^\dagger\eta + 1)(\eta^2 + 1)^{3/2}} ; \quad (61b)$$

$$\Phi_2^{(\text{ext})}(\eta) = \frac{(y^\dagger)^2[2(y^\dagger)^2 - 3]}{[(y^\dagger)^2 + 1]^{7/2}} \ln \frac{[y^\dagger - \eta + \sqrt{(y^\dagger)^2 + 1}\sqrt{\eta^2 + 1}]}{(y^\dagger\eta + 1)[y^\dagger + \sqrt{(y^\dagger)^2 + 1}]} ; \quad (61c)$$

$$P^{(\text{ext})}(\eta) = (y^\dagger)^5\eta^2(2\eta^2 + 3) - (y^\dagger)^4\eta(4\eta^2 + 5) - (y^\dagger)^3(12\eta^4 + 21\eta^2 + 11) - (y^\dagger)^2\eta(3\eta^2 + 5) + y^\dagger(\eta^4 + 6\eta^2 + 4) + \eta^3 ; \quad (61d)$$

using Eqs. (23b), (39), (40), (51), and (52), the HP macrogases equation of state is obtained from the particularization of Eq. (26) to the case of interest for the domain, $y \geq 1$.

In absence of truncation radius, the density drops to zero when the radius goes to infinity, $\Xi \rightarrow +\infty$, $\eta \rightarrow +\infty$, and Eqs. (38)-(40), (50)-(52), reduce to (44)-(46), (55)-(57), respectively, and Eqs. (60)-(61) reduce to:

$$\lim_{\eta \rightarrow +\infty} w^{(\text{int})}(\eta) = -\frac{64\sqrt{2}y^\dagger}{3[(y^\dagger)^2 + 1]^3} \left\{ [(y^\dagger)^4 - 4(y^\dagger)^3 - 12(y^\dagger)^2 + 11y^\dagger + 2] \right.$$

$$-\frac{3y^\dagger[3(y^\dagger)^2 - 2]}{\sqrt{(y^\dagger)^2 + 1}} \ln \frac{\sqrt{(y^\dagger)^2 + 1} - 1}{y^\dagger [y^\dagger + \sqrt{(y^\dagger)^2 + 1}]} \Bigg\} ; \quad y^\dagger \neq 1 ; \quad (62a)$$

$$\lim_{\eta \rightarrow +\infty} w^{(\text{int})}(\eta) = \frac{8}{3} \left[2\sqrt{2} + 3 \ln \frac{\sqrt{2} - 1}{\sqrt{2} + 1} \right] ; \quad y^\dagger = 1 ; \quad (62b)$$

$$\lim_{\eta \rightarrow +\infty} w^{(\text{ext})}(\eta) = -\frac{64\sqrt{2}}{3[(y^\dagger)^2 + 1]^3} \left\{ [2(y^\dagger)^4 + 11(y^\dagger)^3 - 12(y^\dagger)^2 - 4y^\dagger + 1] \right. \\ \left. - \frac{3(y^\dagger)^2[-2(y^\dagger)^2 + 3]}{\sqrt{(y^\dagger)^2 + 1}} \ln \frac{\sqrt{(y^\dagger)^2 + 1} - 1}{y^\dagger [y^\dagger + \sqrt{(y^\dagger)^2 + 1}]} \right\} \quad y^\dagger \neq 1 ; \quad (63a)$$

$$\lim_{\eta \rightarrow +\infty} w^{(\text{ext})}(\eta) = \frac{8}{3} \left[2\sqrt{2} + 3 \ln \frac{\sqrt{2} - 1}{\sqrt{2} + 1} \right] ; \quad y^\dagger = 1 ; \quad (63b)$$

where, in particular, the related expression of the tidal energy coincides with its counterpart calculated in an earlier attempt (Valentinuzzi, 2006, Chap. 4, §4.2.2). Using Eqs. (23b) and (45), (46), (56), (57), (60), (61), the HP macro-gases equation of state in the special situation under discussion, is obtained from the particularization of Eq. (26) to the case of interest, for the domain, $y \geq 0$.

3.5 HN macrogases

The inner density profile (Hernquist, 1990) implies $(\alpha, \beta, \gamma) = (1, 4, 1)$, which is defined by Eq. (49), and related functions and parameters by Eqs. (50)-(52) or (55)-(57) in the special case of no truncation radius.

The outer density profile (Navarro et al., 1995, 1996, 1997) implies $(\alpha, \beta, \gamma) = (1, 3, 1)$, and Eq. (27) reduces to:

$$f_u(\xi_j) = \frac{4}{\xi_j(1 + \xi_j)^2} ; \quad 0 \leq \xi_j \leq \Xi_j ; \quad (64)$$

which, together with its H counterpart expressed by Eq. (49), have been proved to be consistent with nonnegative distribution functions, in the parameter range of interest (Lowenstein and White, 1999).

The particularization of Eqs. (17a), (18b), and (20c) to the case of interest yields:

$$F_j(\xi_j) = \frac{8}{1 + \xi_j} - \frac{8}{1 + \Xi_j} ; \quad (65)$$

$$(\nu_j)_{\text{mas}} = 12 \left[\ln(1 + \Xi_j) - \frac{\Xi_j}{1 + \Xi_j} \right] ; \quad (66)$$

$$(\nu_j)_{\text{sel}} = 36 \frac{\Xi_j(2 + \Xi_j) - 2(1 + \Xi_j) \ln(1 + \Xi_j)}{(1 + \Xi_j)^2} ; \quad (67)$$

with regard to the tidal potential-energy terms, the particularization of Eqs. (24a) and (24b) to the case of interest yields:

$$w^{(\text{int})}(\eta) = -\frac{64y^\dagger}{(y^\dagger - 1)^3} \left[-\frac{(y^\dagger - 1)^2 y^\dagger \eta (y^\dagger \eta + 2)}{y^\dagger (y^\dagger \eta + 1)^2} + \frac{2y^\dagger \eta (y^\dagger - 1)}{y^\dagger \eta + 1} \right. \\ \left. + 2 \ln \frac{\eta + 1}{y^\dagger \eta + 1} - \frac{(y^\dagger - 1)^3}{1 + \Xi_j} \frac{\eta^2}{(y^\dagger \eta + 1)^2} \right] ; \quad y^\dagger \neq 1 ; \quad (68a)$$

$$w^{(\text{int})}(\eta) = -\frac{64\eta^2}{(\eta + 1)^2} \left[\frac{\eta + 3}{3(\eta + 1)} - \frac{1}{1 + \Xi_j} \right] ; \quad y^\dagger = 1 ; \quad (68b)$$

$$w^{(\text{ext})}(\eta) = -\frac{64}{(y^\dagger - 1)^2} \left\{ -\frac{\eta}{\eta + 1} - \frac{y^\dagger \eta}{y^\dagger \eta + 1} - \frac{y^\dagger + 1}{y^\dagger - 1} \ln \frac{\eta + 1}{y^\dagger \eta + 1} \right. \\ \left. - \frac{(y^\dagger - 1)^2}{(1 + \Xi_i)^2} \left[-\frac{\eta}{\eta + 1} + \ln(\eta + 1) \right] \right\} ; \quad y^\dagger \neq 1 ; \quad (69a)$$

$$w^{(\text{ext})}(\eta) = -64 \left\{ \frac{1}{6} \frac{\eta^2(\eta + 3)}{(\eta + 1)^3} - \frac{1}{(1 + \Xi_i)^2} \left[-\frac{\eta}{\eta + 1} + \ln(\eta + 1) \right] \right\} ; \\ y^\dagger = 1 ; \quad (69b)$$

using Eqs. (23b), (51), (52), (66), and (67), the HN macrogases equation of state is obtained from the particularization of Eq. (26) to the case of interest for the domain, $y \geq 1$.

In absence of truncation radius, the density drops to zero when the radius goes to infinity, $\Xi \rightarrow +\infty$, $\eta \rightarrow +\infty$, and Eqs. (50)-(52), reduce to (55)-(57), respectively, and Eqs. (65)-(69) reduce to:

$$\lim_{\Xi_j \rightarrow +\infty} F_j(\xi_j) = \frac{8}{1 + \xi_j} ; \quad (70)$$

$$\lim_{\Xi_j \rightarrow +\infty} (\nu_j)_{\text{mas}} = +\infty ; \quad (71)$$

$$\lim_{\Xi_j \rightarrow +\infty} (\nu_j)_{\text{sel}} = 36 ; \quad (72)$$

$$\lim_{\eta \rightarrow +\infty} w^{(\text{int})}(\eta) = -\frac{64}{(y^\dagger - 1)^3} \left[\frac{(y^\dagger)^2 - 1}{y^\dagger} - 2y^\dagger \ln y^\dagger \right] ; \quad y^\dagger \neq 1 ; \quad (73a)$$

$$\lim_{\eta \rightarrow +\infty} w^{(\text{int})}(\eta) = -\frac{64}{3} ; \quad y^\dagger = 1 ; \quad (73b)$$

$$\lim_{\eta \rightarrow +\infty} w^{(\text{ext})}(\eta) = -\frac{64}{(y^\dagger - 1)^2} \left[2 - \frac{y^\dagger + 1}{y^\dagger - 1} \ln y^\dagger \right] ; \quad y^\dagger \neq 1 ; \quad (74a)$$

$$\lim_{\eta \rightarrow +\infty} w^{(\text{ext})}(\eta) = -\frac{32}{3} ; \quad y^\dagger = 1 ; \quad (74b)$$

where the self potential-energy profile factor remains finite, although the mass profile factor undergoes a logarithmic divergence. Using Eqs. (23b) and (72)-(69), the HN macrogases equation of state (where M_j^\dagger and m^\dagger appear instead of M_j and m) in the situation under consideration, is obtained from the particularization of Eq. (26) to the case of interest, for the domain, $y \geq 0$.

4 Results

The macrogases equation of state, Eq. (26), is represented in the next figures for a number of cases analysed in Section 3. In particular, owing to Eqs. (34) and (35), the UU macrogases equation of state is independent of the scaled truncation radii, (Ξ_i, Ξ_j) .

The macrogases equation of state in absence of truncation radius, is plotted in Fig.1 for cases (from top left in clockwise sense) UU, PP, HH, HP, where $\Xi_j = \Xi_i$ and (from bottom to top in each panel) $m = 1, 2, \dots, 6$, for cases UU, PP, HP, and $m = 10, 20, \dots, 60$, for case HH. Shallower density profiles (UU, PP) show the occurrence of two extremum points: one minimum on the left and one maximum on the right, for arbitrary values of the fractional mass, m . Steeper density profiles (HP, HH) still exhibit extremum points, but none below a threshold, where the critical isofractional mass curve shows a single horizontal inflexion point.

As already noticed in an earlier attempt (CS90), the same trend is shown by van der Waals' (1873) isothermal curves and, in fact, the van der Waals' equation of state looks similar to the macrogases equation of state, Eq. (26), where three variables also appear. Thick curves represent the locus of minimum (left branch) and maximum (right branch) points. The critical isofractional mass curve, when it appears, is also thickened.

A main feature is that, above the critical isofractional mass curve, for any selected value of m , a range in fractional virial potential energy, ϕ , exists, $\phi_{\min} < \phi < \phi_{\max}$, where three different configurations i.e. different fractional truncation radius, y , correspond to the same value of ϕ . By analogy with van der Waals' isothermal curves, it could be argued the existence of a bell-shaped region in the $Oy\phi$ plane, within which the extremum points are located, and

where a phase transition occurs. Further investigation is needed on this point, but it lies outside the aim of the current paper.

The macrogases equation of state in presence of truncation radius, is plotted in Figs. 2 and 3, respectively, for different choices of the fractional truncation radii, (Ξ_i, Ξ_j) , represented on each panel where (from bottom to top) $m = 10, 20, \dots, 60$, and approximate values of the parameters related to the critical point i.e. the horizontal inflexion point on the critical isofractional mass curve (marked by a St. Andrew's cross), are listed in Tab. 1.

It can be seen that the occurrence of the truncation radius makes little change to the trend of the isofractional mass curves. In general, decreasing the outer scaled truncation radius, Ξ_j , yields more pronounced extremum points and vice versa. Much smaller changes, in the same sense, are produced by decreasing the inner scaled truncation radius, Ξ_i . This is why, in the cases under discussion, the mass of the outer subsystem is dominant with respect to the mass of the inner subsystem, $m \gg 1$. The critical isofractional mass curve does not appear for earlier truncated HN density profiles, $(\Xi_i, \Xi_j) = (5, 5)$, which are shallower in comparison with their latter truncated counterparts.

Reduced truncation radii, $\Xi = R/r^\dagger$, may be conceived as concentrations of the related matter distribution (e.g., Navarro et al., 1997; CM03; Caimmi et al., 2005) and the selected range, $5 \leq \Xi \leq 20$, is consistent with the results of dark matter (hereafter quoted as DM) halo numerical simulations (e.g., Bullock et al., 2001) and elliptical galaxy (hereafter quoted as EG) observations (e.g., Lowenstein and White, 1999).

5 Application to elliptical galaxies and their hosting haloes

According to current cosmological scenarios (e.g., Mota and van de Bruck, 2004; Percival, 2005; Horellou and Berge, 2005; Maor and Lahav, 2005; Nunes and Mota, 2006), density perturbations at recombination epoch ($z \approx 1100$) initially expand with the universe, turn around, collapse, and finally virialize (at least in their inner and denser regions).

Virialized density perturbations, such as typical elliptical galaxies (EGs) and clusters of galaxies, may be idealized, to a first extent, as two homeoidally striated, similar and similarly placed, density profiles. In the following, attention shall be focused on EGs.

Table 1: Approximate values of parameters related to the critical point i.e. the horizontal inflexion point on the critical isofractional mass curve, for the density profiles under investigation. Bars instead of numbers mean absence of critical curve in the corresponding case. Numbers in brackets denote the values of scaled truncation radii, (Ξ_i, Ξ_j) . In absence of truncation radius, $\Xi \rightarrow +\infty$, the case considered is $\Xi_j/\Xi_i \rightarrow 1$, which implies $y^\dagger = y$. For homogeneous configurations (case UU) the isofractional mass curves are independent of (Ξ_i, Ξ_j) .

case	(Ξ_i, Ξ_j)	m^\dagger	m	y^\dagger	y	φ
HN	(05-05)	—	—	—	—	—
	(05-10)	04.41	09.45	1.04	2.08	09.16
	(05-20)	05.14	15.49	1.14	4.56	13.44
	(10-05)	03.17	03.68	0.88	0.44	03.90
	(10-10)	06.36	11.46	1.38	1.38	11.48
	(10-20)	07.24	18.33	1.50	3.00	16.47
	(20-05)	04.99	05.27	1.18	0.29	05.75
	(20-10)	08.10	13.30	1.62	0.81	13.74
	(20-20)	09.10	20.99	1.75	1.75	19.48
HH	(05-05)	07.10	07.10	2.32	2.32	06.86
	(05-10)	07.72	09.19	2.43	4.86	08.17
	(05-20)	07.90	10.32	2.45	9.80	08.62
	(10-05)	11.15	09.37	3.18	1.59	09.44
	(10-10)	11.88	11.88	3.30	3.30	11.03
	(10-20)	12.10	13.28	3.33	6.66	11.57
	(20-05)	15.00	11.50	3.77	0.94	12.04
	(20-10)	15.83	14.42	3.88	1.94	13.94
	(20-20)	16.08	16.08	3.92	3.92	14.60
	$(\infty-\infty)$	20.22	20.22	4.27	4.27	18.15
HP	$(\infty-\infty)$	04.59	04.59	2.05	2.05	06.03
PP	$(\infty-\infty)$	—	—	—	—	—
UU	(Ξ_i, Ξ_j)	—	—	—	—	—

5.1 General considerations and main assumptions

A recent investigation performed on an optically complete sample of 42 EGs, for which X-ray gas temperatures and central stellar velocity dispersions were determined (Davis & White 1996), has shown evidence that, in general, EGs contain substantial amounts of DM (Loewenstein and White, 1999). Accordingly, more than about 20% and 39%-85% of the total mass within one and six optical radii, respectively, is in form of (non baryonic) DM, depending on the stellar density profile and observed value of X-ray gas temperature and central stellar velocity dispersion. The comparison between the velocity dispersion distributions for DM and stars, assuming isotropic orbits, shows that the DM is dynamically “hotter” than the stars, by a factor 1.4-2 (Loewenstein and White, 1999).

The above investigation cannot be considered as conclusive in favour of the existence of DM haloes hosting EGs. In fact, it has been pointed out that the attenuation (in particular, the scattering) by dust grains has the same effect on the stellar kinematics as a DM halo (Baes and Dejonghe, 2001). According to a recent attempt, no strong evidence for DM haloes within 1-3 optical radii has been found in a restricted sample of 4 early-type EGs, using dynamical modelling (Samurovic and Danziger, 1995). Beyond 1-3 optical radii, the X-ray methodology shows the need of DM where an X-ray halo is detected (Samurovic and Danziger, 1995). A similar trend is exhibited by an additional early-type EG (Samurovic and Danziger, 1996). In any case, current cosmological scenarios (Λ CDM, QCDM) predict DM haloes hosting EGs, as well as spiral galaxies, for which there are lots of empirical evidence (e.g., flat rotation curves well outside optical radii). For this reason, EGs are also assumed to be embedded within DM haloes.

An analysis on the evolution of the physical properties of cosmological baryons at low redshifts ($z \lesssim 5$) has recently been performed (Valageas et al., 2002), which (i) yields robust model-independent results that agree with numerical simulations; (ii) recovers the fraction of matter within different phases and the spatial clustering computed by numerical simulations; (iii) predicts a soft X-ray background due to the “warm” intergalactic medium component, that is consistent with observations. The related baryon fraction in the present universe is found to be 7% in hot gas, 24% in the warm intergalactic medium, 38% in the cool intergalactic medium, 9% within star-like objects and, as a still unobserved component, 22% of dark baryons associated with collapsed structures, with a relative uncertainty no larger than 30% on these numbers. Then the amount of still undetected baryons is about one fifth of the total, one fourth of the observed baryons (intergalactic medium, stellar components, and hot gas), and at least twice the stellar-like compo-

nent.

According to recent investigations, HH (e.g., Ciotti, 1996) or HN (e.g., Loewenstein and White, 1999) models provide viable representations for the inner, baryonic, and the outer, nonbaryonic subsystem, respectively. The above mentioned mass distributions were found to be self-consistent, in the parameter range of interest, with regard to the non negativity of the distribution function (e.g., Ciotti, 1996; Loewenstein and White, 1999) by use of a theorem stated in an earlier attempt (Ciotti and Pellegrini, 1992).

If undetected baryons in EGs are present as hot gas, the gaseous subsystem is expected to be less concentrated than the stellar one, as in the Coma cluster of galaxies (e.g., Briel et al. 1992). If undetected baryons in EGs are present as unseen stars, the undetected subsystem is expected to be as concentrated as the stellar one. Either assumption is necessary in dealing with two-component systems. The real situation lies between the above mentioned limiting cases.

The typical velocity dispersion components, deduced by use of the virial theorem (hereafter referred to, in general, as the virial velocity dispersions) are global quantities, related to the virial potential energy of the subsystem as a whole, and so, by construction, independent of the specific orbital distribution of the particles. This important property, however, is also a weakness of the virial theorem, in dealing with velocity dispersion components measured in the central region of a galaxy. In fact, it is well known that the related values can be significantly different for structurally identical subsystems (and so characterized by identical virial velocity dispersion components), due to different orbital structures (e.g., de Zeeuw & Franx 1991). When using central velocity dispersion components, an approach based on Jeans equations (even though still questionable) is to be preferred (e.g., Ciotti et al., 1996; Ciotti & Lanzoni 1997; Loewenstein and White, 1999). On the other hand, a comparison between the results obtained by use of either above mentioned methods, may provide additional support to both of them and/or useful indications on the nature of the problem under investigation.

Strictly speaking, the central velocity dispersions (along the line of sight) in EGs, which are deduced from observations, should be scaled to the virial velocity dispersions. Both observational evidence (e.g., Gerhard et al. 2001) and theoretical arguments (e.g., Nipoti et al. 2002) point towards the existence of dynamical homology in EGs. In particular, a linear relation is found between a local parameter, averaged central velocity dispersion, and a global parameter, inferred maximum circular velocity, $\sigma_{0.1} = (2/3)(v_c)_{max}$ (Gerhard et al. 2001). Accordingly, the central velocity dispersion components are expected to be proportional to the virial velocity dispersion components. Then it could be assumed that the related proportionality factor is of the order of

unity.

In fact, typical peculiar velocity component distributions within EGs show a maximum which is rapidly attained in the central region (at about 1 kpc), and a slow decrease occurs moving outwards (no more than about 13% the maximum at about 10 kpc), at least in the case of isotropic orbits; for further details see related attempts (e.g., Loewenstein and White, 1999). Accordingly, both the central and the virial velocity dispersion components are expected to be of comparable order, slightly less than the maximum of the peculiar velocity component distribution (e.g., Cappellari et al., 2006). On the other hand, most EGs are moderately radially anisotropic (e.g., Gerhard et al. 2001), and the related variation in central velocity dispersion (an increase for increasing σ_i^2 and vice versa) is also expected to be moderate.

5.2 Input parameters, specific assumptions, and results

The main assumptions of the current model are (i) homeoidally striated density profiles and (ii) similar and similarly placed boundaries. Aspherical, heterogeneous, self-gravitating fluids in dynamical or hydrostatic equilibrium exhibit isopycnic surfaces different from ellipsoids (e.g., Chandrasekhar, 1933; Chandrasekhar and Lebovitz, 1962; Vandervoort and Welty, 1981; Lai et al., 1993), and the above assumption (i) is due to reasons of simplicity.

Axisymmetric configurations with nonsimilar boundaries have been investigated in the special case of homogeneous density profiles i.e. UU macrogases, where the shape of one component is kept fixed and an additional variable, the axis ratio of the other component, together with an additional relation, the angular momentum conservation of the other component, must be considered (CS90). A main feature is that the isofractional mass curves on the $(Oy\phi)$ plane cannot converge to 0 at $y \rightarrow +\infty$, as the ending point occurs when the inner subsystem attains a flat configuration. For further details refer to the parent paper (CS90). Being the calculations for heterogeneous density profiles much more complicated, the above assumption (ii) is also due to reasons of simplicity. It can be expected that the effect due to nonsimilar boundaries is maximum for homogeneous density profiles, and decreases as the profile is steeper, to be null for mass points surrounded by a massless atmosphere (Roche ellipsoids). Then the results found for homogeneous density profiles (CS90) make a valid reference for inhomogeneous density profiles. In conclusion, the above assumptions (i) and (ii) are related to a viable model which can be used for specific applications to large-scale celestial objects, in particular EGs.

Given a typical EG, a natural question (in the light of the model under discussion) arises about its position on the $(Oy\phi)$ plane for assigned density profiles and specified input parameters. Towards this aim, the following main assumptions are made: (a) the stellar and the DM distributions are described by homeoidally striated, similar and similarly placed, HH or HN density profiles, respectively; (b) undetected baryons trace either DM haloes or EGs; and (c) the virial theorem holds for each subsystem within the tidal potential of the other one.

According to the above assumptions, a typical EG embedded in a DM halo is idealized as two homeoidally striated, similar and similarly placed matter distributions, where the star and non baryonic subsystem are described by HH or HN density profiles, respectively.

For assigned density profiles, the macrogases equation of state, Eq. (26), depends on two independent variables: the fractional truncation radius, $y = R_j/R_i$, and the fractional mass, $m = M_j/M_i$, or their scaling counterparts, $y^\dagger = r_j^\dagger/r_i^\dagger$ and $m^\dagger = M_j^\dagger/M_i^\dagger$. To represent celestial objects in the $(Oy\phi)$ plane, two additional equations are requested. Having in mind an application to EGs and their hosting haloes, denoted in the following by the index i and j , respectively, for $y \geq 1$, an additional relation between the stellar projected velocity dispersion, $(\sigma_i)_{R_e/8}$, averaged over the aperture used for spectroscopic observations ($r = R_e/8$), and the fractional scaling radius, y^\dagger , may be deduced from the virial theorem related to the star subsystem, Eq. (8b), by solving the appropriate Jeans equations, following an earlier approach (Ciotti et al., 1996). The result may be written as:

$$(\sigma_i)_{R_e/8}^2 = \frac{GM_i}{r_i^\dagger} \psi_i(y^\dagger, m^\dagger) \quad ; \quad (75)$$

where ψ_i is a function calculated by a numerical algorithm.

Using Eq. (75) implies further restrictions, as its validity is limited to (i) spherical-symmetric matter distributions; (ii) isotropic peculiar velocity distributions; (iii) infinite truncation radii; (iv) HH density profiles. Concerning points (i)-(iii) mentioned above, acceptable approximations may safely be expected. On the other hand, HH density profiles provide a viable description to EGs embedded within DM haloes (e.g., Ciotti, 1996).

At this stage, an additional relation is needed. The mere existence of a fundamental plane (Djorgovski and Davis, 1987; Dressler et al., 1987) indicates that structural properties in EGs span a narrow range, suggesting that some self-regulating mechanism must be at work during formation and evolution. In particular, projected light profiles from EGs exhibit large degree of homogeneity and may well be fitted by the $r^{1/4}$ de Vaucouleurs law.

Accordingly, a narrow range may safely be expected also for EG fractional mass and the assumption, $m = \text{const}$, appears to be a viable approximation. The last, together with Eqs. (26) and (75), makes a system of three equations in the three unknowns, ϕ , y , m , via Eqs. (21), for HH density profiles. Then the position of EGs and their hosting haloes on a selected isofractional mass curve in the $(Oy\phi)$ plane, can be determined.

The sample used ($N = 16$) is extracted from a larger sample ($N = 25$) of EGs and lenticular galaxies investigated within the SAURON project (Cappellari et al., 2006, Tab.1 therein), for which the parameters of interest i.e. masses, projected central velocity dispersions, and effective radii, can be derived from the data listed in Tab.2. More specifically, with regard to the inner (stellar) subsystem, projected central velocity dispersions are deduced from the luminosity-weighted second moment of the line-of-sight velocity distribution within the effective radius, σ_e , as $(\sigma_i)_{R_e/8} = 8^{0.066}\sigma_e$; masses are deduced from luminosities and mass-luminosity ratios (in I -band), as $M_i/M_{10} = (L/L_\odot)[(M_i/L)/(10^{10}m_\odot/L_\odot)]$; $L/L_\odot = \exp_{10}\{-0.4[I_T - (\hat{m} - \hat{M}) - 4.11]\}$; scaling radii are calculated from effective radii (in arcsec) and distances, by use of a profile factor, equal to 1.81, related to the case under discussion (Hernquist, 1990), as $r_i^\dagger/\text{kpc} = (R_e/\text{kpc})/1.81$; $R_e/\text{kpc} = [(R_e/\text{arcsec})(d/\text{Mpc})]/206.265$; $d/\text{Mpc} = \exp_{10}[(\hat{m} - \hat{M})/5 - 5]$. For further details refer to the parent paper (Cappellari et al., 2006).

The substitution of the selected value of the fractional mass, m , into Eq. (75), allows the value of the fractional scaling radius, y^\dagger , for each sample object. Finally, the substitution of (y^\dagger, m) values into Eq. (26), particularized to HH density profiles via Eqs. (56)-(59), allows the value of the fractional virial potential energy, ϕ , and the position of each sample object on a selected isofractional mass curve in the $(Oy\phi)$ plane, can be determined.

The results are plotted for different choices of scaled truncation radii, (Ξ_i, Ξ_j) , and different choices of fractional masses, m , in Fig. 4. Isofractional mass curves, $m = 10$ (top panels), and $m = 20$ (bottom panels), are labelled by the selected choices of scaled truncation radii, (Ξ_i, Ξ_j) , indicated near the corresponding curves, and the sample objects are represented as dots. Curves lie above and below the critical curve for $m = 10$, while all curves lie above the critical curve for $m = 20$, with respect to the cases considered.

The above description is due to reasons of simplicity, but the model does not necessarily imply that sample objects must be located on the same isofractional mass curve and/or correspond to the same scaled truncation radii. What is relevant is the position of EGs on the $(Oy\phi)$ plane, which implies the following assumptions: (i) there are in the universe 16 EGs with intrinsic values of the parameters equal to their counterparts listed in Tab. 2 for sample objects, and (ii) related star distributions are well described by H

Table 2: Data related to a subsample ($N = 16$) extracted from a sample ($N = 25$) of EGs and lenticular galaxies investigated within the SAURON project (Cappellari et al., 2006), and deduced values of the parameters of interest. Column caption: (1) NGC number; (2) effective (half-light) radius, R_e , measured in the I -band; (3) total observed I -band galaxy magnitude; (4) mass-luminosity ratio (including DM) deduced from the best fitting three-integral Schwarzschild model, computed at a fiducial inclination; (5) mass-luminosity ratio of the stellar population; (6) galaxy distance modulus (hats avoid confusion with the fractional mass, m , and the total mass, M); (7) galaxy mass, calculated as $M_i/M_{10} = (L/L_\odot)[(M_i/L)/(10^{10}m_\odot/L_\odot)]$; $L/L_\odot = \exp_{10}\{-0.4[I_T - (\hat{m} - \hat{M}) - 4.11]\}$; (8) galaxy central velocity dispersion, deduced from the luminosity-weighted second moment of the line-of-sight velocity distribution within the effective radius, σ_e , as $(\sigma_i)_{R_e/8} = 8^{0.066}\sigma_e$; (9) galaxy scaling radius, calculated as $r_i^\dagger/\text{kpc} = (R_e/\text{kpc})/1.81$; $R_e/\text{kpc} = [(R_e/\text{arcsec})(d/\text{Mpc})]/206.265$; $d/\text{Mpc} = \exp_{10}[(\hat{m} - \hat{M})/5 - 5]$. The factor, 1.81, is related to an assumed Hernquist profile for the inner subsystem (Hernquist, 1990). The factor, 206.265, is related to the choice of measure units. For further details refer to the parent paper (Cappellari et al., 2006).

NGC	R_e	I_T	M/L	M_i/L	$(\hat{m} - \hat{M})$	M_i	$(\sigma_i)_{R_e/8}$	r_i^\dagger
(1)	(arcsec)	(mag)	(I -band)	(I -band)	(mag)	(M_{10})	(km s^{-1})	(kpc)
(1)	(2)	(3)	(4)	(5)	(6)	(7)	(8)	(9)
0821	039.0	09.47	3.08	2.60	31.85	10.26	216.80	2.45
2974	024.0	09.43	4.52	2.34	31.60	07.61	267.28	1.34
3377	038.0	08.98	2.22	1.75	30.19	02.35	158.30	1.11
3379	042.0	08.03	3.36	3.08	30.06	08.80	230.57	1.16
3608	041.0	09.40	3.71	2.57	31.74	09.77	204.19	2.45
4278	032.0	08.83	5.24	3.05	30.97	09.64	264.98	1.34
4374	071.0	07.69	4.36	3.08	31.26	36.35	318.90	3.40
4458	027.0	10.68	2.28	2.27	31.12	01.50	097.50	1.21
4473	027.0	08.94	2.91	2.88	30.92	07.86	220.24	1.10
4486	105.0	07.23	6.10	3.33	30.97	45.97	341.84	4.40
4552	032.0	08.54	4.74	3.35	30.87	12.62	289.07	1.28
4621	046.0	08.41	3.03	3.12	31.25	18.80	242.04	2.19
4660	011.0	09.96	3.63	2.96	30.48	02.11	212.21	0.37
5813	052.0	09.12	4.81	2.97	32.48	28.89	263.83	4.36
5845	004.6	11.10	3.72	2.96	32.01	03.02	274.16	0.31
5846	081.0	08.41	5.30	3.33	31.92	37.19	273.01	5.25

density profiles.

In fact, observational uncertainties on the quantities of interest (Cappellari et al., 2006) make large errors on the fractional scaling radius, y^\dagger . As an example, a single galaxy, NGC 3379, and a single parameter, the effective radius, shall be considered. In the case under discussion, $R_e = (42.0 \pm 7.1)$ arcsec (Cappellari et al., 2006), but different estimates exist, such as (54.8 ± 3.5) arcsec (Capaccioli et al., 1990) which is consistent with the above result within $2\sigma_{R_e}$. Using the latter value, the fractional scaled radius, y^\dagger , passes from 5.74 to 4.08 for a fractional mass, $m = 10$, and from 8.45 to 6.07 for $m = 20$.

Different values of parameters, m , Ξ_i , Ξ_j , makes sample objects locate on different isofractional mass curves, as shown in Fig. 4, where y depends on m but is independent of Ξ_i and Ξ_j . Fiducial values of the above mentioned parameters, say $10 \leq m \leq 20$, $5 \leq \Xi_u \leq 20$, $u = i, j$, define a region on the $(Oy\phi)$ plane, approximately as: $2.5 < y^\dagger < 6.0$, $7 < \phi < 11$, $m = 10$; $4 < y^\dagger < 9$, $17 < \phi < 23$, $m = 20$; where sample objects are positioned, as shown in Fig. 5. Dots and asterisks correspond to inner scaled truncation radii, $\Xi_i = 5$ and 10, respectively. Small and large symbols represent sample objects and configurations where the virial potential energy of the inner subsystem attains the maximum value with respect to a frozen outer subsystem, respectively. No such configuration exists in the cases considered, for fractional masses, $m \lesssim 20$. The related parameter space is restricted to a region close to the angle defined by the locus of large dots and asterisks, respectively. The intersection between the above mentioned loci occurs for outer scaled truncation radii, Ξ_j , slightly larger than 10. The change of position for NGC 3379, due to a change in effective radius, from $R_e = 42.0$ to $R_e = 54.8$, is indicated by squares, regardless of the vertical scale.

In the special situation where the outer subsystem remains frozen and the inner one is free to contract or to expand, with unchanged mass and density profile, the virial potential energy of the inner subsystem may attain an extremum point of maximum (Secco, 2000, 2001, 2005; Marmo and Secco, 2003). For HH density profiles, lower fractional masses ($m = 10$) yield no extremum point, while the contrary holds for larger fractional masses ($m = 20$). The special configurations related to the maximum virial potential energy of the inner subsystem, when the outer subsystem remains frozen (hereafter quoted as “the maximum configuration”), are represented as large dots in Fig. 4 (bottom panels) and large dots and asterisks in Fig. 5.

The maximum configuration appears to have little relevance in the light of the current model for a number of reasons. First, it occurs for fractional masses above a threshold. Second, the loci of maximum configurations on the $(Oy\phi)$ plane show no correlation with the parameter space of the model

related to sample objects. More precisely, the loci of maximum configurations are narrower and extend from bottom left to top right, while sample objects lie on a broader and less inclined band, as shown in Fig. 5.

The position of the maximum configuration on the isofractional mass curves, $m = 20$, depends on the concentration of the outer subsystem, while the position of sample objects can only be vertically shifted, as the fractional scaling radius, y^\dagger , is independent of the concentration, via Eq. (75). In this view, it is difficult to conceive maximum configurations as ending points of any evolutionary track on the $(Oy\phi)$ plane, even if observational uncertainties are high.

EG position on the $(Oy\phi)$ plane, in particular along an isofractional mass curve ($m = \text{const}$), represents the ending point of evolutionary tracks on the above mentioned plane. The related configurations may be thought of as virialized to a good extent, in that sample objects listed in Tab. 2 show no sign of ungoing merger and star formation burst. The coincidence of ending points with maximum configurations would imply, for fixed (m, Ξ_i, Ξ_j) : (i) a single ending point for all sample objects i.e. homologous evolution, and (ii) m above the threshold for the occurrence of maximum configurations, which does not necessarily happen, as shown in Fig. 4. On the contrary, the evolution of EGs appears to be non homologous, in the sense that different ending points take place along the selected isofractional mass curves defined by the HH macrogases equation of state.

Owing to Eqs. (9b) and (12b), the total energy of the virialized system reads:

$$E = \frac{1}{2}[(E_{ij})_{\text{vir}} + (E_{ji})_{\text{vir}}] = -(E_i)_{\text{kin}} - (E_j)_{\text{kin}} ; \quad (76)$$

and the combination of Eqs. (12b), (25), and (76) yields:

$$E = \frac{1}{2}(1 + \phi)(E_{ij})_{\text{vir}} = -(1 + \phi)(E_i)_{\text{kin}} ; \quad \phi = \frac{(E_j)_{\text{kin}}}{(E_i)_{\text{kin}}} ; \quad (77)$$

where the kinetic energy of the inner subsystem, $(E_i)_{\text{kin}}$, may be deduced from observations, and the related total energy, E , may be read on the vertical axis of Fig. 4. Within the range, $\phi_{\text{min}} \leq \phi \leq \phi_{\text{max}}$, three configurations exist with same virial potential (or kinetic) energy ratio, ϕ , and fractional mass, m , but different fractional truncation radius, y .

The restriction to constant fractional mass also in time, makes evolutionary tracks on the $(Oy\phi)$ plane locate on the related isofractional mass curve, ($m = \text{const}$), where displacements from the left to the right (increasing y values) are due to energy dissipation, and displacements from the right to the left (decreasing y values) are due to energy acquisition. In the former alternative, changes in ϕ and $(E_{ij})_{\text{vir}}$ must act to yield a decreasing E (increasing

in absolute value), the larger energy change being related to the larger y change. For further details refer to Appendix B. In this view, the maximum configuration corresponds to a special energy change, $(\Delta E)_{\max}$, and to a special y change, $(\Delta y)_{\max}$. But there is no apparent reason for which a special amount of energy has to be dissipated starting from the beginning of evolution, to attain the maximum configuration. A similar result holds in the latter alternative. In fact, it can be seen in Fig. 4 that the sample objects show no connection with the maximum configuration. Then the maximum configuration, which implies a frozen outer subsystem, has no special relevance in the light of the current model. For an analysis of different theories on the maximum configuration, refer to a specific study (Valentinuzzi 2006, Chaps. 3-5).

The above results hold if the baryonic subsystem is mainly in form of stars. Let us take into consideration a different scenario, where a less concentrated gaseous subsystem than the stellar one is also present, as in the Coma cluster of galaxies (e.g., Briel et al., 1992), and assume the same mass distribution as in the non baryonic matter to preserve use of two-component models (Caimmi, 2003). Accordingly, a typical EG is idealized as formed by an inner subsystem made of stars and an outer subsystem made of gas and non baryonic matter. As the amount of baryonic and non baryonic matter have to remain unchanged, the inner and the outer subsystem are less and more massive, respectively, than in absence of undetected baryons. Again, it is assumed that the related mass distributions are represented by HH density profiles. Then a similar procedure may be followed, keeping in mind that the fractional mass, m , is the ratio of nonbaryonic + extragalactic gas mass to star mass. For further details refer to an earlier attempt (CM03).

6 Conclusion

Two-component systems have been conceived as (two-component) macro-gases, and the related equation of state has been formulated using the virial theorem for subsystems (Limber, 1959; Brosche et al., 1983; Caimmi et al., 1984; Caimmi and Secco, 1992), under the restriction of (i) homeoidally striated ellipsoids (Roberts, 1962) and (ii) similar and similarly placed boundaries.

Explicit calculations have been performed for a useful reference case and a few cases of astrophysical interest, both in presence and in absence of truncation radius. More specifically, the following cases have been dealt with: IJ= UU, PP, HH, HP, HN, where I and J denote the inner and the outer density profile, respectively, and the other captions relate to the following

density profiles: U ($\rho = \text{const}$), P (Plummer, 1911), H (Hernquist, 1990), N (Navarro et al., 1995, 1996, 1997). Shallower density profiles (UU, PP), have been found to yield an equation of state, $\phi = \phi(y, m)$, characterized by the occurrence of two extremum points, one maximum and one minimum, as in an earlier attempt (CS90). Steeper density profiles (HH, HP, HN), have been found to produce a similar equation of state where, in addition, a single horizontal inflexion point occurs in a critical isofractional mass curve, and isofractional mass curves related to lower values, $m = M_j/M_i < m_{\text{crit}}$, show no extremum point. The similarity between isofractional mass curves and van der Waals' isothermal curves, has suggested the possibility that a phase transition could take place in a bell-shaped region of the ($Oy\phi$) plane.

Further investigation has been devoted to HH density profiles for which a numerical algorithm (Ciotti et al., 1996) has been used to represent EGs and their hosting DM haloes along selected isofractional mass curves on the ($Oy\phi$) plane, under the assumption that the related fractional mass has the same value in different systems. In the light of the model, the evolution of EGs has been found to be non strictly homologous, in the sense that the end of evolutionary tracks on the ($Oy\phi$) plane occur at different points along the related isofractional mass curve, instead of being close to a single point.

7 Acknowledgements

We are indebted to an anonymous referee for critical comments which improved an earlier version of the manuscript. Thanks are due to L. Secco for fruitful discussions. The analytical integrations needed in the current paper were helped substantially by use of the Mathematica package and visiting the internet site: "HTTP://INTEGRALS.WOLFRAM.COM/INDEX.CGI". This is why we are deeply grateful to the Wolfram staff, in particular to Daniel Lichtblau, and wish to acknowledge all the facilities encountered therein.

References

- [1] Baes, M., Dejonge, H., 2001. ApJ 563, L19.
- [2] Bett, P., Eke, V., Frenk, C., et al., 2007. MNRAS 376, 215.
- [3] Briel, U.G., Henry, J.P., Böhringer, H., 1992. A&A 259, L31.
- [4] Binney, J., Tremaine, S., 1987. *Galactic Dynamics*, Princeton University Press, Princeton.

- [5] Brosche, P., Caimmi, R., Secco, L., 1983. A&A 125, 338.
- [6] Bullock, J.S., Kolatt, T.S., Sigad, J., et al., 2001. MNRAS 321, 559.
- [7] Caimmi, R., 1986. A&A 159, 147.
- [8] Caimmi, R., 1992. AN 313, 165.
- [9] Caimmi, R., 1993. ApJ 419, 615.
- [10] Caimmi, R., 1995. ApJ 441, 533.
- [11] Caimmi, R., 1996. AN 317, 401.
- [12] Caimmi, R., 2003. AN 324, 250.
- [13] Caimmi, R., 2006a. AN 327, 925.
- [14] Caimmi, R., 2006b. App. Math. Comp. 174, 447.
- [15] Caimmi, R., 2006c. SerAJ 173, 13.
- [16] Caimmi, R., 2007a. SerAJ 174, 13.
- [17] Caimmi, R., 2007b. NewA 12, 327.
- [18] Caimmi, R., 2007c. arXiv:0710.3826.
- [19] Caimmi, R., Secco, L., Brosche, P., 1984. A&A 139, 411.
- [20] Caimmi, R., Secco, L., 1990. A&A 237, 336 (CS90).
- [21] Caimmi, R., Secco, L., 1992. ApJ 395, 119.
- [22] Caimmi, R., Secco, L., 2003. AN 324, 491.
- [23] Caimmi, R., Marmo, C., 2003. NewA 8, 119 (CM03).
- [24] Caimmi, R., Marmo, C., 2004. SerAJ 169, 11.
- [25] Caimmi, R., Marmo, C., 2005. AN 326, 465.
- [26] Caimmi, R., Marmo, C., Valentinuzzi, T., 2005. SerAJ 170, 13.
- [27] Capaccioli, M., Held, E.V., Lorenz, H., et al., 1990. AJ 99, 1813.
- [28] Cappellari, M., Bacon, R., Bureau, M., et al., 2006. MNRAS 366, 1126.
- [29] Carlberg, R.G., Yee, H.K.C., Ellingson, E., et al., 1996. ApJ 462, 32.

- [30] Chandrasekhar, S., 1933. MNRAS 93, 390.
- [31] Chandrasekhar, S., 1939. *An Introduction to the Study of the Stellar Structure*, University of Chicago Press.
- [32] Chandrasekhar, S., Lebovitz, N., 1962. ApJ 136, 1082.
- [33] Chandrasekhar, S., 1969. *Ellipsoidal Figures of Equilibrium*, Yale University Press, New Haven.
- [34] Ciotti, L., 1996. ApJ 471, 68.
- [35] Ciotti, L., 1999. ApJ 520, 574.
- [36] Ciotti, L., Pellegrini, S., 1992. MNRAS 255, 561.
- [37] Ciotti, L., Lanzoni, B., Renzini, A., 1996. MNRAS 282, 1.
- [38] Ciotti, L., Lanzoni, B., 1997. A&A 321, 724.
- [39] Clausius, R., 1870. *Sitz. Niederrheinischen Gesellschaft*, Bonn, p.114 [translated in Phil. Mag. 40, 112 (1870)].
- [40] Davis, D.S., White, R.E., III, 1996. ApJ 470, L35.
- [41] de Zeeuw, T., Franx, M., 1991. ARA&A 29, 239.
- [42] Djorgovski, S.G., Davis, M., 1987. ApJ 313, 59.
- [43] Dressler, A., Lynden-Bell, D., Burstein, D., et al., 1987. ApJ 313, 42.
- [44] Emden, R., 1907. *Gas Kugeln*, Leipzig.
- [45] Gerhard, O., Kronawitter, A., Saglia, R.P., Bender, R., 2001. AJ 121, 1936.
- [46] Girardi, M., Giuricin, G., Mardirossian, F., et al., 1998. ApJ 505, 74.
- [47] Hernquist, L., 1990. ApJ 356, 359.
- [48] Horedt, G.P., 2004. *Polytropes*, ApSS Library, vol. 306, Kluwer Acad. Publ.
- [49] Horellou, C., Berge, J., 2005. MNRAS 360, 1393.
- [50] Lai, D., Rasio, F.A., Shapiro, S.L., 1993. ApJS 88, 205.
- [51] Landau, L., Lifchitz, E., 1966. *Mecanique*, Mir, Moscow.

- [52] Lane, J.H., 1870. Amer. J. Sci. Arts 50, 57.
- [53] Limber, D.N., 1959. ApJ 130, 414.
- [54] Lowenstein, M., White, R.E., III, 1999. ApJ 518, 50.
- [55] MacMillan, W.D., 1930. *The Theory of the Potential*, Dover Publications, New York, 1958.
- [56] Marmo, C., Secco, L., 2003. NewA 8, 629.
- [57] Maor, I, Lahav, O., 2005. JCAP 7, 3.
- [58] Mota, D.F., van de Bruck, C., 2004. A&A 421, 71.
- [59] Mouri, H., Taniguchi, Y., 2003. ApJ 585, 250.
- [60] Navarro, J.F., Frenk, C.S., White, S.D.M., 1995. MNRAS 275, 720.
- [61] Navarro, J.F., Frenk, C.S., White, S.D.M., 1996. ApJ 462, 563.
- [62] Navarro, J.F., Frenk, C.S., White, S.D.M., 1997. ApJ 490, 493.
- [63] Neutsch, W., 1979. A&A 72, 339.
- [64] Nipoti, C., Londrillo, P., Ciotti, L., 2002. MNRAS 332, 901.
- [65] Nunes, N.J., Mota, D.F., 2006. MNRAS 368, 751.
- [66] Percival, W.J., 2005. A&A 443, 819.
- [67] Plummer, H.C., 1911. MNRAS 71, 460.
- [68] Roberts, P.H., 1962. ApJ 136, 1108.
- [69] Samurovic, S., Danziger, I.J., 2005. MNRAS 363, 769.
- [70] Samurovic, S., Danziger, I.J., 2006. A&A 458, 79.
- [71] Schuster, A., 1883. Brit. Ass. Rep., p.428.
- [72] Secco, L., 2000. NewA 5, 403.
- [73] Secco, L., 2001. NewA 6, 339.
- [74] Secco, L., 2005. NewA 10, 349.

- [75] Spiegel, M.R., 1968. *Mathematical Handbook*, Schaum's Outline Series, McGraw-Hill, Inc., New York.
- [76] The, L.S., White, S.D.M., 1986. AJ 92, 1248.
- [77] Valageas, P., Schaeffer, R., Silk, J., 2002. A&A 388, 741.
- [78] Valentinuzzi, T., 2006. Unpublished PHD Thesis, Padua University.
- [79] Vandervoort, P.O., 1980. ApJ 240, 478.
- [80] Vandervoort, P.O., Welty, D.E., 1981. ApJ 248, 504.
- [81] van der Waals, J.D., 1873. *Over de Continuïteit van den Gas-en Vloeistoftoestand* (Doctoral Thesis).
- [82] Zhao, H.S., 1996. MNRAS 278, 488.

Appendix

A Plummer density profiles and $n = 5$ polytropes

The Lane-Emden equation reads (e.g., Lane, 1870; Emden, 1907; Chandrasekhar, 1933; Horedt, 2004, Chap. 2, §2.1):

$$\frac{1}{\xi_{\text{LE}}^2} \frac{d}{d\xi_{\text{LE}}} \left(\xi_{\text{LE}}^2 \frac{d\theta}{d\xi_{\text{LE}}} \right) = -\theta^n ; \quad (78a)$$

$$\theta(0) = 1 ; \quad \theta(\Xi_{\text{LE}}) = 0 ; \quad (78b)$$

$$\xi_{\text{LE}} = \frac{r}{\alpha_{\text{LE}}} ; \quad \Xi_{\text{LE}} = \frac{R}{\alpha_{\text{LE}}} ; \quad (78c)$$

$$\rho(r) = \lambda \theta^n(\xi_{\text{LE}}) ; \quad (78d)$$

where n is the polytropic index ($0 \leq n \leq 5$ and $0.5 < n \leq 5$ for realistic collisional and collisionless equilibrium configurations, respectively), α_{LE} is a scaling radius and λ is the central density.

In the special case, $n = 5$, the integration of Eq.(78a) yields (Schuster, 1883; see also Chandrasekhar, 1939, Chap. IV, §4; Horedt, 2004, Chap. 2, §2.3.3):

$$\theta(\xi_{\text{LE}}) = \left(1 + \frac{1}{3} \xi_{\text{LE}}^2 \right)^{-1/2} ; \quad \Xi_{\text{LE}} \rightarrow +\infty ; \quad n = 5 ; \quad (79a)$$

$$\frac{d\theta}{d\xi_{\text{LE}}} = -\frac{1}{3}\xi_{\text{LE}} \left(1 + \frac{1}{3}\xi_{\text{LE}}^2\right)^{-3/2} ; \quad (79b)$$

$$-\xi_{\text{LE}}^2 \frac{d\theta}{d\xi_{\text{LE}}} = \sqrt{3} \left(\frac{\xi_{\text{LE}}}{\sqrt{3}}\right)^3 \left[1 + \left(\frac{\xi_{\text{LE}}}{\sqrt{3}}\right)^2\right]^{-3/2} ; \quad (79c)$$

$$\lim_{\xi_{\text{LE}} \rightarrow +\infty} \left(-\xi_{\text{LE}}^2 \frac{d\theta}{d\xi_{\text{LE}}}\right) = \sqrt{3} ; \quad (79d)$$

and the general expression of a polytrope mass (e.g., Chandrasekhar, 1939, Chap. IV, §4; Horedt, 2004, Chap. 2, §2.6.3):

$$M = -4\pi\lambda\alpha_{\text{LE}}^3 \Xi_{\text{LE}}^2 \left(\frac{d\theta}{d\xi_{\text{LE}}}\right)_{\Xi_{\text{LE}}} ; \quad (80)$$

in the case of interest, using Eqs. (79), reduces to:

$$M = \sqrt{3} 4\pi\lambda\alpha_{\text{LE}}^3 ; \quad n = 5 ; \quad (81)$$

finally, the explicit expression of the density profile results from the combination of Eqs. (78d) and (79a), as:

$$\rho(r) = \lambda \left(1 + \frac{1}{3}\xi_{\text{LE}}^2\right)^{-5/2} ; \quad n = 5 ; \quad (82)$$

and the following relation is derived from comparison with Eqs. (14a) and (27):

$$\rho^\dagger 2^\chi \xi^{-\gamma} (1 + \xi^\alpha)^{-\chi} = \lambda \left(1 + \frac{1}{3}\xi_{\text{LE}}^2\right)^{-5/2} ; \quad (83)$$

which, in turn, implies the following:

$$\xi = \frac{\xi_{\text{LE}}}{\sqrt{3}} ; \quad \alpha_{\text{LE}} = \frac{\xi}{\xi_{\text{LE}}} r^\dagger = \frac{r^\dagger}{\sqrt{3}} ; \quad (84a)$$

$$\gamma = 0 ; \quad \alpha = 2 ; \quad \chi = \frac{5}{2} = \frac{\beta - \gamma}{\alpha} = \frac{\beta}{2} ; \quad \beta = 5 ; \quad (84b)$$

$$\lambda = 2^{5/2} \rho^\dagger ; \quad (84c)$$

and the substitution of Eqs. (84a) and (84c) into (82) yields:

$$\rho(r) = \rho^\dagger f(\xi) ; \quad (85a)$$

$$f(\xi) = \frac{2^{5/2}}{(1 + \xi^2)^{5/2}} ; \quad (85b)$$

according to Eq. (37).

An equivalent formulation can be obtained by the combination of Eqs. (81) and (84). The result is:

$$\rho(r) = \frac{3M}{4\pi} \frac{(r^\dagger)^2}{[r^2 + (r^\dagger)^2]^{5/2}} ; \quad (86)$$

which is known as the Plummer (1911) density profile.

B Quasi static contraction in presence of tidal potential

The scalar virial equations, Eqs. (12b), for assigned density profiles i.e. fixed α_u , β_u , γ_u , and Ξ_u , $u = i, j$, depend on four parameters e.g., masses and scaling radii, M_u and r_u^\dagger . The further assumption of spherical-symmetric matter distributions is only to simplify calculations. Let an assigned amount of energy, $\Delta E < 0$, be instantaneously dissipated within the inner subsystem, as:

$$(E_i)_{\text{kin}} \rightarrow (E_i)_{\text{kin}} + \Delta E ; \quad (87)$$

and the system readjust to attain a new configuration in accordance with Eqs. (12b) where, in general, density profiles and scaling radii are changed, while masses and the outer subsystem truncation radius may be assumed fixed, or their variations assigned. More specifically, density profiles are steepened by energy dissipation, and the system gets bounder i.e. a larger (in absolute value) binding energy is attained.

The further constraint of density profiles unaffected by energy dissipation, implies the following changes ($u = i, j$):

$$M_u \rightarrow M_u + \Delta M_u ; \quad \Delta M_u = 0 ; \quad (88a)$$

$$\Xi_u \rightarrow \Xi_u + \Delta \Xi_u ; \quad \Delta \Xi_u = 0 ; \quad (88b)$$

$$R_u \rightarrow R_u + \Delta R_u ; \quad \Delta R_j = 0 ; \quad (88c)$$

$$r_u^\dagger \rightarrow r_u^\dagger + \Delta r_u^\dagger ; \quad \Delta r_j^\dagger = 0 ; \quad (88d)$$

$$(E_u)_{\text{kin}} \rightarrow (E_u)_{\text{kin}} + \Delta E_u ; \quad \Delta E_i + \Delta E_j = \Delta E ; \quad (88e)$$

where the assumption that energy dissipation within the inner subsystem has no effect on (i) masses, M_u ; (ii) scaled truncation radii, Ξ_u ; density profiles, $(\alpha_u, \beta_u, \gamma_u)$; (iv) truncation radius of the outer subsystem, R_j ; implies a frozen outer subsystem. In general, the changes, $\Delta M_u = \zeta_m M_u$, $\Delta R_u = \zeta_u R_u$, and $\Delta r_u^\dagger = \zeta_u r_u^\dagger$, which make m and Ξ_u conserved, should be specified.

The application of the scalar virial theorem, Eqs.(12), to the subsystems before and after energy dissipation, reads:

$$U_{uv}(y^\dagger) + 2(E_u)_{\text{kin}} = 0 \quad ; \quad (89a)$$

$$U_{uv}(y^\dagger + \Delta y^\dagger) + 2[(E_u)_{\text{kin}} + \Delta E_u] = 0 \quad ; \quad (89b)$$

$$U_{uv} = (E_{uv})_{\text{vir}} \quad ; \quad u = i, j \quad ; \quad v = j, i \quad ; \quad (89c)$$

where the fractional scaling radius, $y^\dagger = r_j^\dagger/r_i^\dagger$, has been chosen as variable.

The combination of Eqs. (89a) and (89b) yields:

$$\Delta(E_{uv})_{\text{vir}} + 2\Delta E_u = 0 \quad ; \quad u = i, j \quad ; \quad v = j, i \quad ; \quad (90a)$$

$$\Delta(E_{uv})_{\text{vir}} = U_{uv}(y^\dagger + \Delta y^\dagger) - U_{uv}(y^\dagger) \quad ; \quad (90b)$$

and the combination of Eqs. (90a), by use of (88e) produces:

$$\Delta(E_{ij})_{\text{vir}} + \Delta(E_{ji})_{\text{vir}} + 2\Delta E = 0 \quad ; \quad (91)$$

which is a transcendental equation in Δy^\dagger provided the density profiles and the amount of dissipated energy, ΔE , are specified. In general, the changes, $\Delta M_u = \zeta_m M_u$, $\Delta R_u = \zeta_u R_u$, and $\Delta r_u^\dagger = \zeta_u r_u^\dagger$, which make m and Ξ_u conserved, should also be specified. Then the remaining parameters related to the relaxed system, due to energy dissipation, may be determined. In particular, $\Delta y^\dagger > 0$ is expected together with $m = \text{const}$ due to mass conservation in each subsystem or mass variation of the kind considered, $m = (M_j + \Delta M_j)/(M_i + \Delta M_i) = M_j/M_i$. Accordingly, the position of the system in the $(Oy\phi)$ plane moves from the left to the right along the related isofractional mass curve (see e.g., Fig. 4).

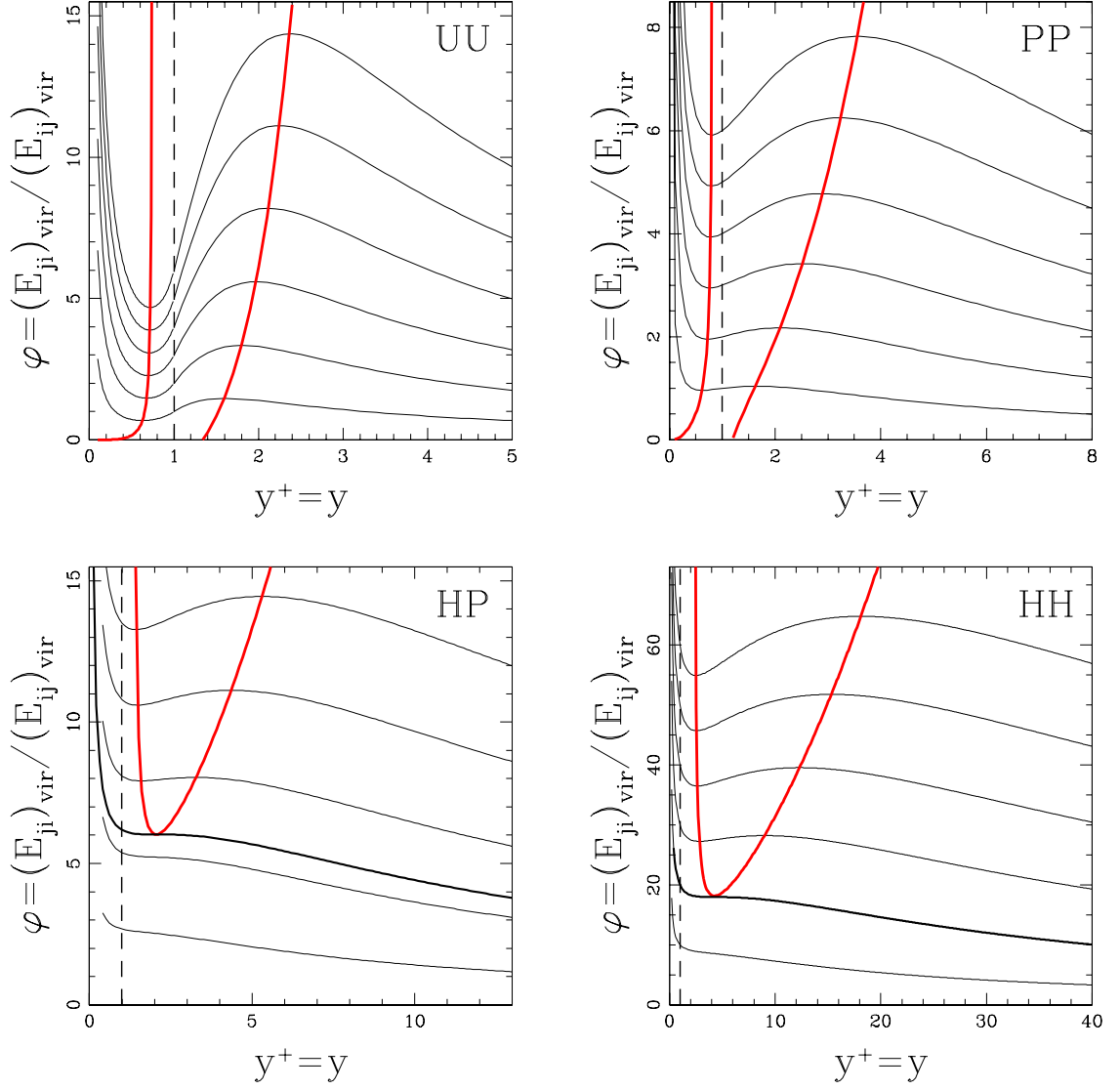


Figure 1: Isofractional mass curves related to (from top left in clockwise sense) UU, PP, HH, HP, macrogases for $\Xi \rightarrow +\infty$, $\Xi_j/\Xi_i \rightarrow 1$. Thick curves represent the locus of minimum (left branch) and maximum (right branch) points. The critical curve is also thickened, and the horizontal inflexion point, or critical point, is defined (when present) as the tangent point with respect to the locus of the extremum points. The value of the fractional mass is $m = \phi(1, m)$ and can be read on the intersection between the selected curve and the dashed vertical line, $y^\dagger = y = 1$, provided the density profile of the inner and the outer subsystem belong to the same family (UU, PP, HH). All the curves diverge at $y \rightarrow 0$ and converge to 0 at $y \rightarrow +\infty$. For UU macrogases, the extremum points of the $m = 0$ isofractional mass curve occur at $y = 0$ and $y = 3/\sqrt{5}$, respectively, and the locus of the minimum points has a vertical asymptote, $y = \sqrt{5}/3$. For PP macrogases, the extremum points of the $m = 0$ isofractional mass curve occur at $y = 0$ and $y \approx 1.20$, respectively, and the locus of the minimum points has a vertical asymptote, $y \approx 0.84$.

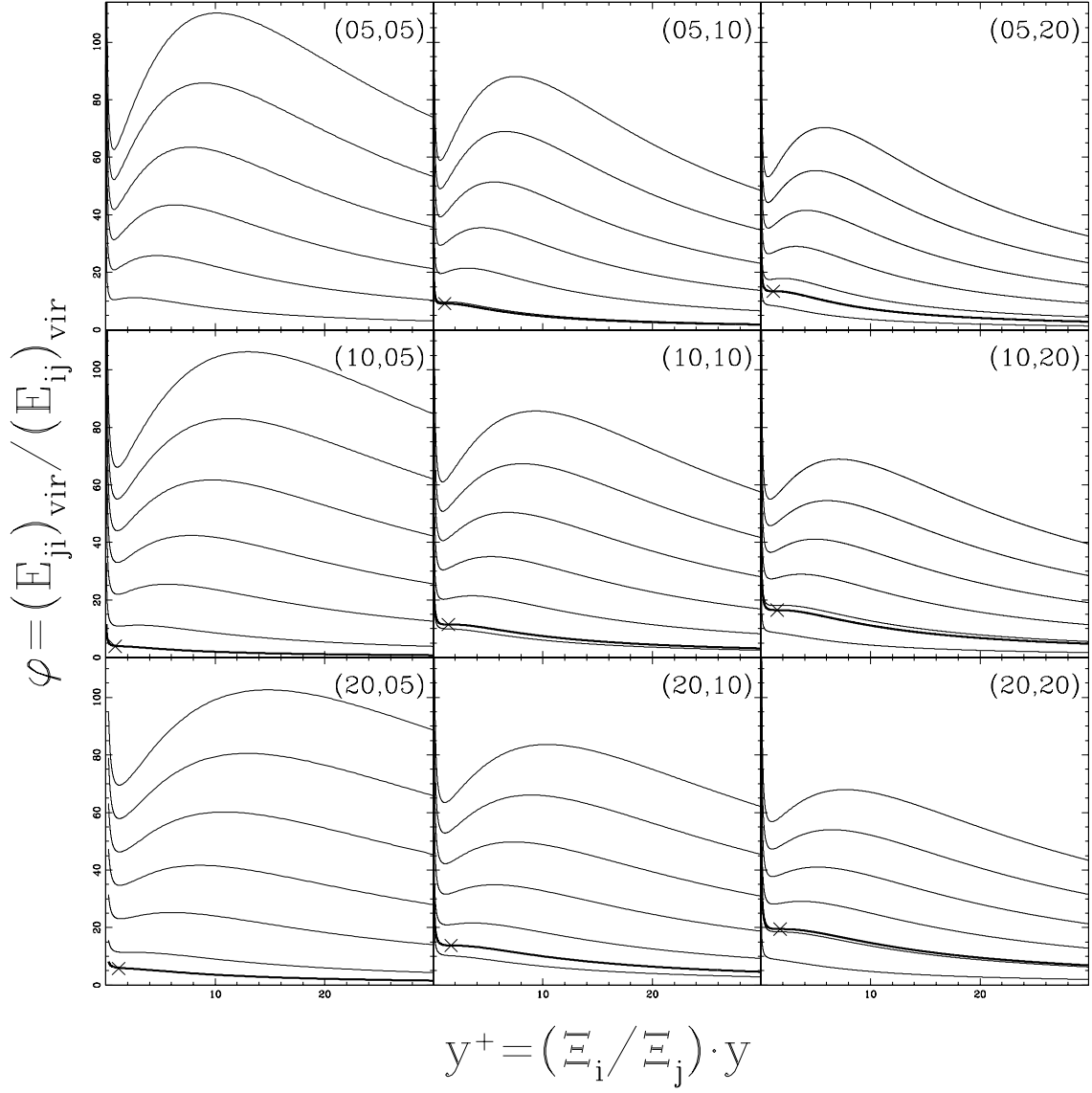


Figure 2: Isofractional mass curves related to HH macrogases, for different choices of scaled truncation radii, (Ξ_i, Ξ_j) , represented on each panel, where (from bottom to top) $m = 10, 20, \dots, 60$. The critical isofractional mass curve, where the horizontal inflexion point, or critical point, is marked by a St. Andrew's cross, is thickened on each panel. All the curves diverge at $y \rightarrow 0$ and converge to 0 at $y \rightarrow +\infty$.

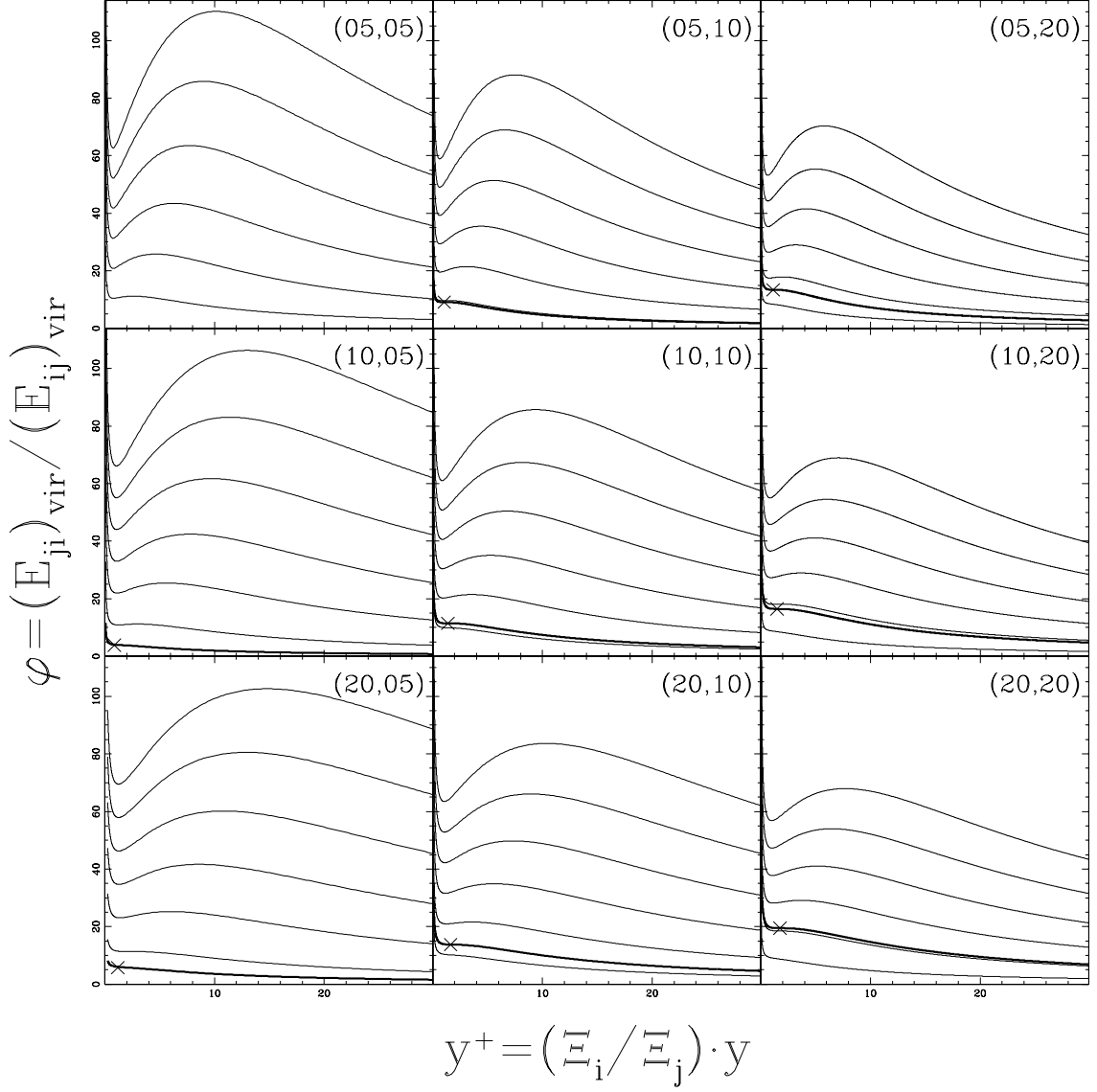


Figure 3: Isofractional mass curves related to HN macrogases, for different choices of scaled truncation radii, (Ξ_i, Ξ_j) , represented on each panel, where (from bottom to top) $m = 10, 20, \dots, 60$. The critical isofractional mass curve, where the horizontal inflexion point, or critical point, is marked by a St. Andrew's cross, is thickened on each panel. All the curves diverge at $y \rightarrow 0$ and converge to 0 at $y \rightarrow +\infty$.

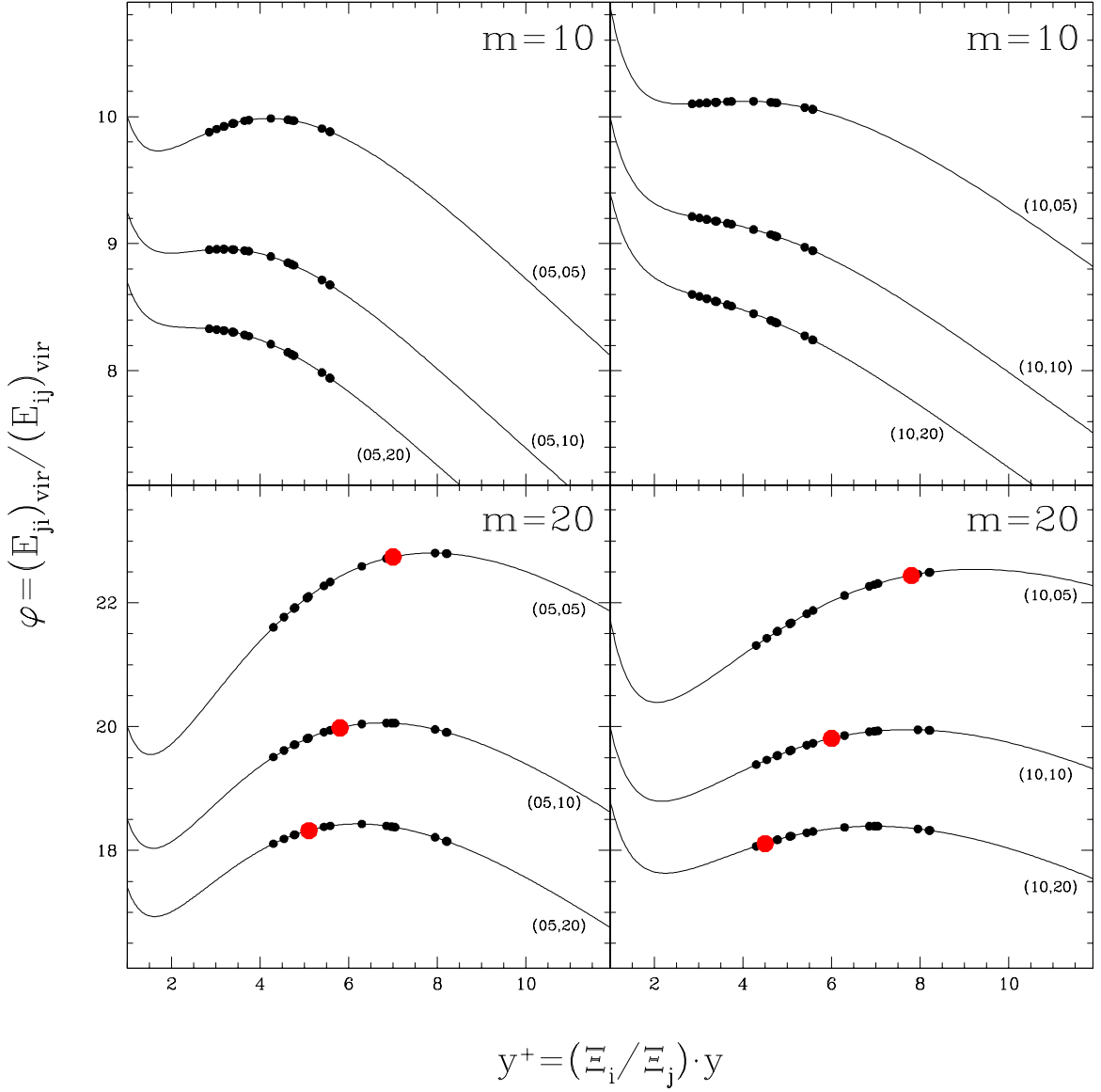


Figure 4: Isofractional mass curves, $m = 10$ (top panels), and $m = 20$ (bottom panels), related to HH macrogases, for different choices of scaled truncation radii, (Ξ_i, Ξ_j) , indicated near the corresponding curves, and related positions of $N = 16$ EGs (dots), listed in Tab. 2. Different cases correspond to vertical shifts of the sample objects. Larger dots represent configurations where the virial potential energy of the inner subsystem attains the maximum value with respect to a frozen outer subsystem.

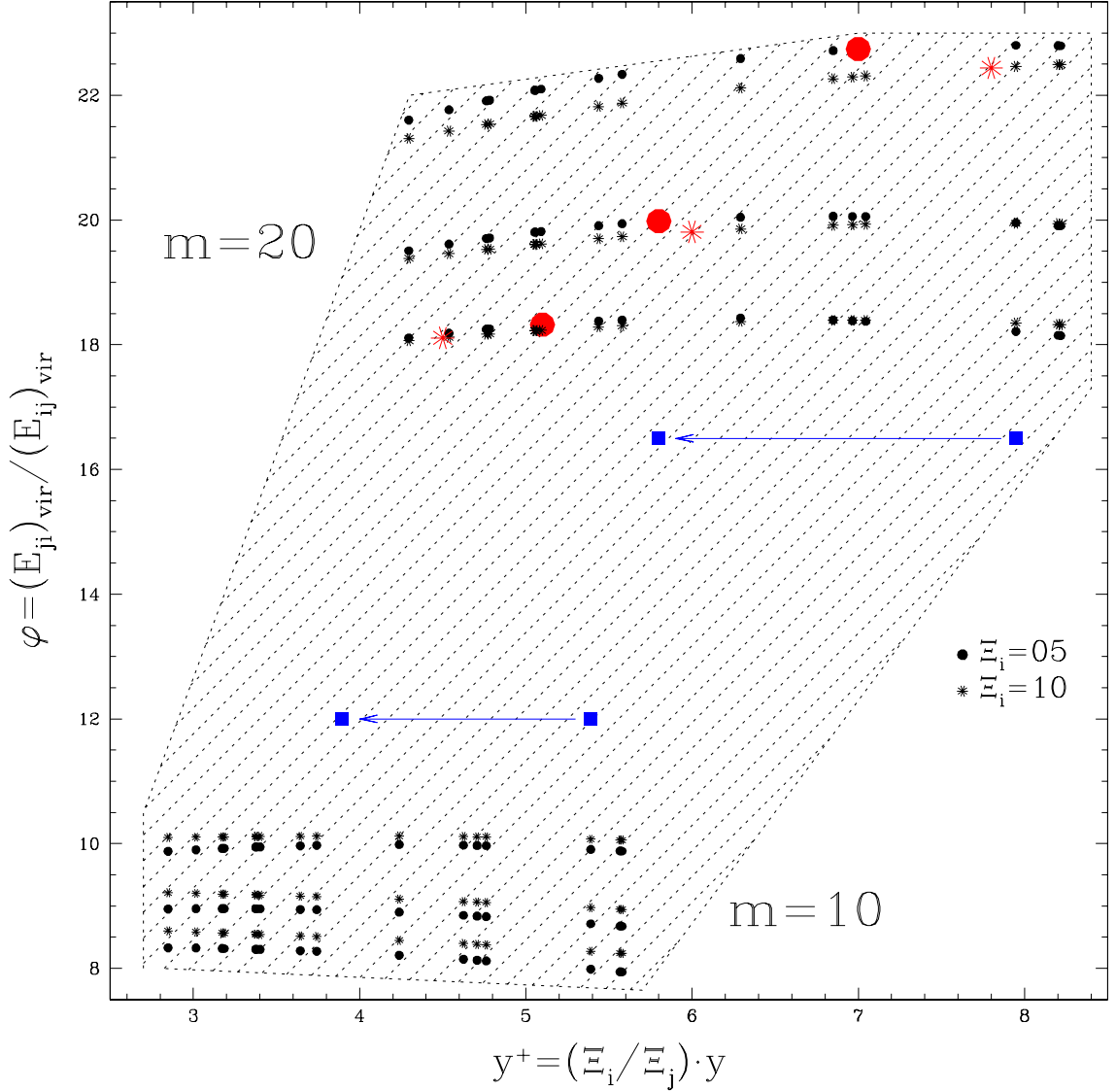


Figure 5: The parameter space of the cases plotted in Fig. 4, roughly outlined by the shaded region. Dots and asterisks correspond to inner scaled truncation radii, $\Xi_i = 5$ and 10 , respectively. For fixed fractional mass, m , the corresponding outer scaled truncation radii read $\Xi_j = 5, 10, 20$, from top to bottom. Small and large symbols represent sample objects and configurations where the virial potential energy of the inner subsystem attains the maximum value with respect to a frozen outer subsystem, respectively. No such configuration exists in the cases considered, for fractional masses, $m \lesssim 20$. The related parameter space is restricted to a region close to the angle defined by the locus of large dots and asterisks, respectively. The intersection between the above mentioned loci occurs for outer scaled truncation radii, Ξ_j , slightly larger than 10 . The change of position for NCG 3379, due to a change in effective radius, from $R_e = 42.0$ to $R_e = 54.8$, is indicated by squares, regardless of the vertical scale.